Journal of Mathematical Imaging and Vision
https://doi.org/10.1007/s10851-020-00959-4

Shape Analysis of Surfaces Using General Elastic Metrics

Zhe Su[1] · Martin Bauer[1] · Stephen C. Preston[2] · Hamid Laga[3,4] · Eric Klassen[1]

Received: 15 October 2019 / Accepted: 9 April 2020

Abstract
In this article, we introduce a family of elastic metrics on the space of parametrized surfaces in 3D space using a corresponding family of metrics on the space of vector-valued one-forms. We provide a numerical framework for the computation of geodesics with respect to these metrics. The family of metrics is invariant under rigid motions and reparametrizations; hence, it induces a metric on the "shape space" of surfaces. This new class of metrics generalizes a previously studied family of elastic metrics and includes in particular the Square Root Normal Field (SRNF) metric, which has been proven successful in various applications. We demonstrate our framework by showing several examples of geodesics and compare our results with earlier results obtained from the SRNF framework.

Keywords Shape spaces · Vector valued one-forms · Elastic metrics · SRNF metric · Surface registration

1 Introduction

Shape analysis of surfaces in $\mathbb{R}^3$ has been motivated by many applications in bioinformatics, computer graphics and medical imaging, see, e.g., [2,14,16,19,22,32]. In most applications, the actual parametrization of the surfaces under consideration is unknown and one is only able to observe the "shape" of the object, i.e., a priori the point correspondences between the surfaces are unknown and should be an output of the performed analysis. Furthermore, we will often identify surfaces that only differ by a rigid motion. Thus, we define the shape space of surfaces as the quotient space of all parametrized surfaces modulo the group of reparametrizations and/or the group of rigid motions. One goal in shape analysis is to quantify the differences and find the optimal deformations between the given objects; see Fig. 1 for two examples of optimal deformations between distinct surfaces.

The main challenge in the context of shape analysis of surfaces consists in the registration problem, i.e., finding the (optimal) point correspondences between distinct surfaces, which can then be used as the basis for the resulting statistical analysis. In the previous work, the correspondence problem has often been solved in a preprocessing step, which is then followed by an independent statistical analysis of the resulting parametrized surfaces. This approach can yield several undesirable consequences on the statistical analysis, see, e.g., [29].

The goal of elastic shape analysis is to formulate this problem in a unified framework: Using a *reparametrization invariant* metric on the space of all parametrized surfaces, one then studies the induced Riemannian metric on the quotient space. Using this approach, the point correspondences

M. Bauer was partially supported by NSF-Grant 1912037 (collaborative research in connection with NSF-Grant 1912030). S. C. Preston was partially supported by Simons Foundation Collaboration Grant for Mathematicians No. 318969. E. Klassen was partially supported by Simons Foundation Collaboration Grant for Mathematicians No. 317865.

✉ Martin Bauer
bauer@math.fsu.edu

Zhe Su
zsu@math.fsu.edu

Stephen C. Preston
stephen.preston@brooklyn.cuny.edu

Hamid Laga
H.Laga@murdoch.edu.au

Eric Klassen
klassen@math.fsu.edu

1 Department of Mathematics, Florida State University, Tallahassee, USA

2 Department of Mathematics, Brooklyn College and CUNY Graduate Center, New York, USA

3 Information Technology, Mathematics and Statistics, Murdoch University, Perth, Australia

4 The Phenomics and Bioinformatics Research Centre, University of South Australia, Adelaide, Australia

Published online: 14 May 2020

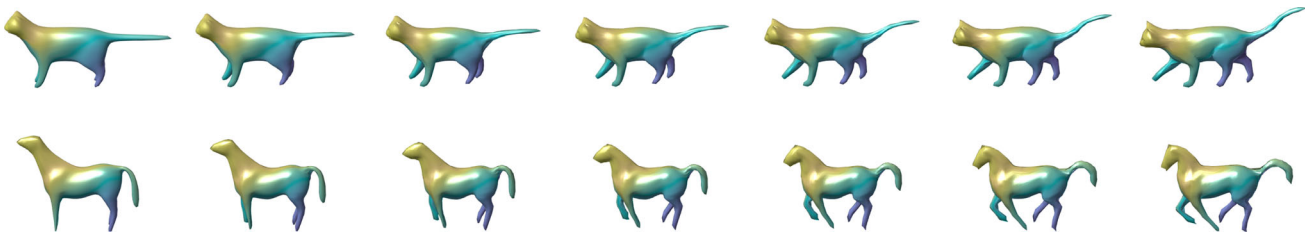

Fig. 1 Geodesics between shapes in the space of unparametrized surfaces $\mathrm{Imm}(S^2, \mathbb{R}^3)/\mathrm{Diff}_+(S^2)$ with respect to the split metric (4) for a choice of coefficients (1, 1, 0.1, 0)

and the resulting statistical analysis can be performed in a consistent way.

In the past years, several metrics and frameworks have been proposed as potential approaches to this goal, see, e.g., [4,18,24,25,29,33]. In particular, a class of elastic metrics has been proposed in [17], which is defined as a weighted sum of three components that measure the differences in shearing, stretching and bending of the surface. This family of metrics is actually a subfamily of the general class of reparametrization invariant Sobolev metrics, as studied in [4–6]. It is also a natural generalization of the family of elastic $G^{a,b}$-metrics on the space of curves [26], which has been proven efficient and successful in numerous shape analysis applications [10,28–31,34–36].

To obtain a numerically efficient representation, Srivastava et al. [28] introduced the so-called Square Root Velocity Function (SRVF) for comparing curves. In this framework, the space of curves endowed with the elastic metric for a particular choice of coefficients is isometric to an L^2-space, which makes the computation of geodesics extremely easy and efficient. Motivated by this progress, Jermyn et al. [18] introduced the Square Root Normal Field (SRNF) representation for elastic shape analysis of surfaces and showed that the L^2-metric on the space of SRNFs corresponds to one member of a more general class of elastic metrics on the space of surfaces. While it is computationally efficient, there are several drawbacks to this approach: The SRNF metric only consists of the last two terms of the general elastic metric for surfaces and is thus highly degenerate; i.e., there exists a high-dimensional space of deformations that has no cost in this framework.[1] Furthermore, the SRNF map is neither injective nor surjective, and its image is not fully understood. In consequence, there exists no analytic formula for geodesics in the image space and geodesics are usually approximated by numerically inverting the straight line between the given SRNFs, where each inversion is calculated as the solution to an optimization problem [25].

[1] See the article [20] for an example of a path of closed surfaces that connects two distinct shapes, such that the whole path has the same SRNF.

Contributions of this article The purpose of the present article is to introduce a numerical framework for the computation of the geodesic initial and boundary value problem with respect to a family of metrics that contains the general elastic metric as a special case. The framework complements [7] which defined, using vector-valued one-forms, a metric on the space of surfaces that is invariant under rigid motions and reparametrizations. It does not require a numerical inversion of the SRNF map and thus overcomes some of the aforementioned difficulties. Furthermore, this framework will allow us in the future to choose the constants of the metric in a data-driven way, which has potential importance in many applications. See [3,23] for related considerations regarding the choice of constants for the elastic metric on the space of curves.

2 Mathematical Framework and Background

In this section, we will give the formal definition of the space of shapes and describe the general elastic metric. Then, we will introduce a new representation for the elastic metric using vector valued one-forms, which will still allow us to obtain an efficient discretization of the geodesic boundary value problem.

From here on, we will model a surface as an immersion f from a model space M into $\mathbb{R}^3$, i.e., a smooth map from M to $\mathbb{R}^3$ that has an injective tangent mapping. Here, M is a two-dimensional compact manifold encoding the topology of the objects under consideration. Typically, choices of M include the two-sphere $M = S^2$ or the sheet $M = [0, 1]^2$.

Denote by $\mathrm{Imm}(M, \mathbb{R}^3)$ the space of all immersions. To define the space of shapes, we now consider the actions of the group of rigid motions and the group of diffeomorphisms on $\mathrm{Imm}(M, \mathbb{R}^3)$. The group of rigid motions is given by the semidirect product of the group of rotations and the group of translations, i.e., $\mathrm{SO}(3) \ltimes \mathbb{R}^3$, where $\mathrm{SO}(3)$ is the set of all rotation matrices. It acts on $\mathrm{Imm}(M, \mathbb{R}^3)$ as follows:

$$\begin{aligned}\left(\mathrm{SO}(3) \ltimes \mathbb{R}^3\right) \times \mathrm{Imm}(M, \mathbb{R}^3) &\to \mathrm{Imm}(M, \mathbb{R}^3)\\ ((R, v), f) &\mapsto Rf + v.\end{aligned}$$

Denote by $\mathrm{Diff}_+(M)$ the group of diffeomorphisms that preserve the orientation of M. The action of $\mathrm{Diff}_+(M)$ on $\mathrm{Imm}(M,\mathbb{R}^3)$ is given by composition from the right:

$$\begin{aligned}\mathrm{Imm}(M,\mathbb{R}^3)\times \mathrm{Diff}_+(M) &\to \mathrm{Imm}(M,\mathbb{R}^3)\\ (f,\gamma) &\mapsto f\circ\gamma.\end{aligned}$$

We say that two immersions f_1 and f_2 have the *same shape* if they are in the same orbit of the action of $\mathrm{Diff}_+(M)$, or both actions depending on whether we want to mod out rigid motions. The space of shapes can then be defined as the quotient space:

$$\mathcal{S}(M,\mathbb{R}^3)=\mathrm{Imm}(M,\mathbb{R}^3)/\mathcal{G},$$

where $\mathcal{G}=\mathrm{Diff}_+(M)$ or $\mathcal{G}=\mathrm{Diff}_+(M)\times(\mathrm{SO}(3)\ltimes\mathbb{R}^3)$.

This quotient space has some mild singularities and does not carry the structure of a smooth manifold but only of an infinite-dimensional orbifold [11]. However, for the purpose of this article, we can ignore these subtleties and assume that we are always working away from the singularities, which allows us to treat $\mathcal{S}(M,\mathbb{R}^3)$ as an infinite-dimensional manifold.

By endowing the space of immersions $\mathrm{Imm}(M,\mathbb{R}^3)$ with a Riemannian metric that is invariant under the actions of $\mathrm{SO}(3)\ltimes\mathbb{R}^3$ and $\mathrm{Diff}_+(M)$, the space of shapes $\mathcal{S}(M,\mathbb{R}^3)$ becomes a Riemannian manifold (orbifold), where the metric is induced by the Riemannian metric on $\mathrm{Imm}(M,\mathbb{R}^3)$.

In the following, we will denote by $\mathrm{dist}_{\mathrm{Imm}}$ the geodesic distance function of a Riemannian metric on the space of immersions $\mathrm{Imm}(M,\mathbb{R}^3)$ and by $[f]$ the equivalence class of f under the action of $\mathcal{G}$. Given two surfaces f_1 and f_2, we can define the distance between $[f_1]$ and $[f_2]$ as the infimum of the distance between the orbits of f_1 and f_2 under the action of $\mathcal{G}$. For example, the distance function on the space of unparametrized surfaces $\mathcal{S}=\mathrm{Imm}(M,\mathbb{R}^3)/\mathrm{Diff}_+(M)$ can be defined as follows:

$$\mathrm{dist}_{\mathcal{S}}([f_1],[f_2])=\inf_{\gamma\in\mathrm{Diff}_+(M)}\mathrm{dist}_{\mathrm{Imm}}(f_1\circ\gamma,f_2).$$

We will use this induced distance as our measure for comparing unparametrized surfaces. Given two parametrized surfaces, to measure the similarity between them, we will need to find the optimal reparametrization in $\mathrm{Diff}_+(M)$ that realizes the infimum. If we also want to mod out rigid motions and find the distance between two elements in the space of unparametrized surfaces modulo rigid motions $\mathrm{Imm}(M,\mathbb{R}^3)/\left(\mathrm{Diff}_+(M)\times\mathrm{SO}(3)\ltimes\mathbb{R}^3\right)$, we will need to solve a joint optimization problem of finding the best reparametrization, rotation and translation.

2.1 The General Elastic Metric and the SRNF Framework

Jermyn et al. introduced in [18] the general elastic metric which has the desired invariance properties under shape-preserving deformations. To define this metric, we first introduce a transformation that maps an immersion onto its induced surface metric and normal vector field:

$$\begin{aligned}\mathrm{Imm}(M,\mathbb{R}^3)&\mapsto \mathrm{Met}(M)\times C^\infty(M,\mathbb{R}^3)\\ f&\to\left(g:=g^f,n:=n^f\right),\end{aligned}$$

where n^f is the unit normal vector field to the surface f, which is given in local coordinates by

$$n=\frac{f_x\times f_y}{|f_x\times f_y|}$$

and where the surface metric is given by

$$g=f^*\langle .,.\rangle_{\mathbb{R}^3}=\langle Tf.,Tf.\rangle_{\mathbb{R}^3}.$$

It is classical result in Riemannian geometry that any surface can be reconstructed uniquely by these two quantities [1]. Thus, this representation allows one to define a Riemannian metric on the space of immersions by describing it on the image $\mathrm{Met}(M)\times C^\infty(M,\mathbb{R}^3)$. The general elastic metric as introduced in [18] is defined by:

$$\begin{aligned}&G_{g,n}((\delta g,\delta n),(\delta g,\delta n))\\ &\quad=A\int_M \mathrm{tr}(g^{-1}\delta g g^{-1}\delta g)\mu_g+B\int_M\mathrm{tr}(g^{-1}\delta g)^2\mu_g\\ &\qquad+C\int_M\langle\delta n,\delta n\rangle_{\mathbb{R}^3}\mu_g\end{aligned}\tag{1}$$

where $A,B,C\geq 0$ are constants and where μ_g denotes the induced volume density of the surface f.

Each of the three terms appearing in the metric (1) has a natural geometric interpretation: The first term penalizes local change in the metric (shearing), the second term measures the change in the volume density (scaling) and the third term quantifies the change in the normal vector (bending).

Instead of using the (g,n) representation for comparing surfaces, in the same paper [18], Jermyn et al. introduced the SRNF framework, where a surface is represented only as a rescaled normal vector field:

$$\begin{aligned}\mathcal{Q}:\mathrm{Imm}(M,\mathbb{R}^3)&\to C^\infty(M,\mathbb{R}^3)\\ f(s)&\mapsto\sqrt{A(s)}n(s),\end{aligned}$$

where $A(s)$ denotes the local area-multiplication factor, which is given in local coordinates by $A(s)=|f_x(s)\times f_y(s)|$.

After equipping the target space $C^\infty(M,\mathbb{R}^3)$ with the flat L^2 metric, the map Q becomes an infinitesimal isometry, where the space $\mathrm{Imm}(M,\mathbb{R}^3)$ is equipped with the elastic metric $G^{A,B,C}$ with $A=0$, $B=\frac{1}{16}$ and $C=1$, i.e., the pullback of the L^2 metric on $C^\infty(M,\mathbb{R}^3)$ along the map Q is equal to the metric $G^{0,\frac{1}{16},1}$. Note, however, that the resulting metric is degenerate for this choice of constants, i.e., there might exist deformation fields that have no cost with respect to the metric. Furthermore, given $q\in C^\infty(M,\mathbb{R}^3)$, there may be either no preimage $Q^{-1}(q)\in\mathrm{Imm}(M,\mathbb{R}^3)$ of q or many preimages. Most importantly, the image of the space of immersions under the SRNF map cannot be easily characterized and, so far, it is not well understood.

Although the distance between two surfaces, which is given by the L^2 difference between their SRNFs, can be easily calculated, finding the inversion of the linear path between their SRNFs that realizes this distance is not possible as the linear path will usually leave the image of the SRNF representation. In [25], Laga et al. introduced a way to approximate the inversion of arbitrary paths between SRNFs by formulating inversion as an optimization problem. In practice, this has been used to approximate geodesics, by numerically inverting straight lines between the SRNFs. However, since the image of the SRNF map is not convex in L^2, this method will not yield geodesics with respect to the SRNF metric, see Table 3.

2.2 Immersions and Vector Valued One-Forms

In the following, we will introduce our framework for comparing surfaces. Therefore, let $\Omega^1(M,\mathbb{R}^3)$ denote the space of all smooth $\mathbb{R}^3$ valued one-forms on M and $\Omega^1_+(M,\mathbb{R}^3)$ denote the subset of $\Omega^1(M,\mathbb{R}^3)$, which contains all full-ranked one-forms on M. Given a metric g on M, in a local chart with a field of orthonormal bases, an element of $\Omega^1_+(M,\mathbb{R}^3)$ can be represented as a field of full-ranked 3×2 matrices. We consider the differential as a mapping

$$\begin{aligned} d:\mathrm{Imm}(M,\mathbb{R}^3)/\mathrm{trans} &\to \Omega^1_+(M,\mathbb{R}^3)\\ f &\mapsto df\ . \end{aligned} \tag{2}$$

The differential d as defined above is injective, but not surjective. Furthermore, in contrast to the SRNF mapping $\mathcal{Q}$ mentioned in Sect. 2.1, it is easy to characterize the image of the differential d. The following theorem contains this characterization and a result concerning the manifold structure space of full-ranked one forms $\Omega^1_+(M,\mathbb{R}^3)$:

Theorem 1 *The space of smooth full-ranked one-forms $\Omega^1_+(M,\mathbb{R}^3)$ is an open subset of an infinite-dimensional vector space of one-forms $\Omega^1(M,\mathbb{R}^3)$, and thus it is an infinite-dimensional Fréchet manifold, where the tangent space at each point is simply $\Omega^1(M,\mathbb{R}^3)$.*

Furthermore, the image of the differential d is the space of all exact full-ranked one-forms, which is the intersection of $\Omega^1_+(M,\mathbb{R}^3)$ with a linear subspace of $\Omega^1(M,\mathbb{R}^3)$.

Proof The proof of this result follows directly from the definition of these spaces. □

This theorem allows us to define a Riemannian metric on these spaces as follows. Let $\alpha\in\Omega^1_+(M,\mathbb{R}^3)$ and $\xi\in T_\alpha\Omega^1_+(M,\mathbb{R}^3)$. For the volume form μ on M induced by the metric g, we let

$$G_\alpha(\xi,\xi)=\int_M \mathrm{tr}\left(\xi_x(\alpha_x^T\alpha_x)^{-1}\xi_x^T\right)\sqrt{\det(\alpha_x^T\alpha_x)}\mu. \tag{3}$$

It is easy to see that the integrand is positive definite, and thus the formula defines a nondegenerated Riemannian metric. This metric does not depend on the choice of orthonormal bases we choose and is actually independent of the metric g on M, see [7] for more details. Thus, we can choose any convenient metric g on M and use it to calculate this metric on $\Omega^1_+(M,\mathbb{R}^3)$.

Using the injection (2), we obtain a pullback metric on the space $\mathrm{Imm}(M,\mathbb{R}^3)$ modulo translations and it turns out that this metric is related to the full elastic metric. The space of immersions equipped with this inner product is an infinite-dimensional Riemannian manifold. It should be noted that, with respect to this metric, $\mathrm{Imm}(M,\mathbb{R}^3)/\mathrm{trans}$ is neither geodesically complete nor geodesically convex. In addition, there exists no explicit formula to calculate minimizing geodesics between two given immersions f_1 and f_2. Instead, we will rely on numerical methods to minimize the path length over all paths of immersions connecting the given immersions f_1 and f_2. Alternatively, these minimizing deformations can be found by solving the Lagrangian optimality condition for the energy functional, called the geodesic equation. Although we will not follow this strategy, we will present this equation in "Appendix A."

First, however, we will orthogonally decompose the tangent space at α in a similar manner as in the definition of the elastic metric earlier. In the following, we will denote the Moore–Penrose inverse of α by α^+, which is defined by $\alpha^+=(\alpha^T\alpha)^{-1}\alpha^T$ where α is a 3×2 matrix of rank 2. Using this notation, we let

$$\xi=\xi_m+\frac{1}{2}\mathrm{tr}(\alpha^+\xi)\alpha+\xi^\perp+\xi_0,$$

where

$$\begin{aligned}\xi_m&=\frac{1}{2}\alpha(\alpha^T\alpha)^{-1}(\alpha^T\xi+\xi^T\alpha)-\frac{1}{2}\mathrm{tr}(\alpha^+\xi)\alpha\\ \xi^\perp&=\xi-\alpha(\alpha^T\alpha)^{-1}\alpha^T\xi\\ \xi_0&=\frac{1}{2}\alpha(\alpha^T\alpha)^{-1}(\alpha^T\xi-\xi^T\alpha)\end{aligned}$$

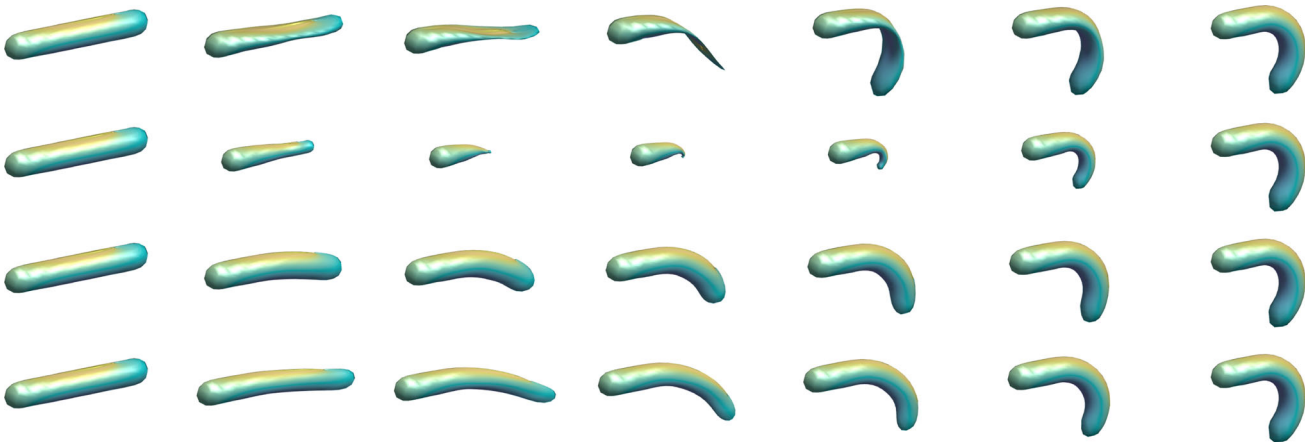

Fig. 2 Geodesics between two cylinders in the space of immersions $\mathrm{Imm}(M, \mathbb{R}^3)$ with respect to different choices of coefficients (from top to bottom): (1, 1, 0, 1), (1, 0, 1, 1), (1, 1, 1, 0), $(0, \frac{1}{2}, 1, 0)$

It is easy to check that these terms are orthogonal with respect to metric (3). We can now obtain a family of metrics on $\Omega^1_+(M, \mathbb{R}^3)$:

$$\begin{aligned} &G_\alpha^{\mathfrak{a},\mathfrak{b},\mathfrak{c},\mathfrak{d}}(\xi,\xi) \\ &\quad = \mathfrak{a}G_\alpha(\xi_m,\xi_m) + \mathfrak{b}G_\alpha\left(\frac{1}{2}\operatorname{tr}(\alpha^+\xi)\alpha, \frac{1}{2}\operatorname{tr}(\alpha^+\xi)\alpha\right) \\ &\qquad + \mathfrak{c}G_\alpha(\xi^\perp,\xi^\perp) + \mathfrak{d}G_\alpha(\xi_0,\xi_0), \end{aligned} \tag{4}$$

where the first summand is measuring the deformation of the metric (within the class of metrics with the same volume form), the second summand is measuring the deformation of the volume density, the third summand is measuring the deformation of the normal vector. The interpretation of the last summand is less intuitive: it measures changes in the one-form that locally come from rotations about the normal vector.

The following theorem shows the connection of our split metric (4) with the elastic metric (1) on surfaces.

Theorem 2 *If $\mathfrak{d} = 0$, then the pullback of the split metric (4) gives rise to the elastic metric (1) on the space of immersions.*

Proof See "Appendix B" for a proof of this result. □

In Fig. 2, we show geodesics between two parametrized cylinders with respect to the split metric (4) for different choices of coefficients $\mathfrak{a}$, $\mathfrak{b}$, $\mathfrak{c}$ and $\mathfrak{d}$. One can see how the choice of coefficients affects the resulting geodesic. Thus, in each specific application, we are now able to adjust the coefficients of the metric in a data-driven way to obtain desired deformations between the shapes under consideration.

Remark 1 In [7], we have presented a detailed study of metric (3) on the space $\Omega^1_+(M, \mathbb{R}^3)$. In particular, we have obtained an explicit formula for the corresponding geodesic initial value problem; in that situation, geodesics can be computed pointwise, so the problem reduces to a finite-dimensional ODE which can be solved explicitly, and gives the solution in the infinite-dimensional context we are dealing with here.

The space of full-ranked exact one-forms $\Omega^1_{+,ex}(M, \mathbb{R}^3)$ is, however, a proper subspace of the space of full-ranked one-forms $\Omega^1_+(M, \mathbb{R}^3)$ and is not a totally geodesic submanifold of $\Omega^1_+(M, \mathbb{R}^3)$ with respect to metric (3). As the space of immersions corresponds to the space of full-ranked exact one-forms, the obtained explicit formula for geodesics does not directly help to calculate geodesics on the space of immersions, which is the main goal of this article. In order to solve the geodesic problem, we will thus introduce a discretization of the metric and solve the geodesic matching problem using path-straightening algorithms.

Note that the split metric (4) is defined on differentials and thus is, by definition, independent of translations. To show the invariance of the split metric under rigid motions and diffeomorphisms, we now consider the action of the group of rotations SO(3) on $\Omega^1_+(M, \mathbb{R}^3)$, which is defined by pointwise left multiplication:

$$\begin{aligned} \mathrm{SO}(3) \times \Omega^1_+(M,\mathbb{R}^3) &\to \Omega^1_+(M,\mathbb{R}^3) \\ (R,\alpha) &\mapsto R\alpha, \end{aligned}$$

where $(R\alpha)_x = R\alpha_x$, and the action of the group of diffeomorphisms $\mathrm{Diff}_+(M)$ on $\Omega^1_+(M, \mathbb{R}^3)$, which is defined via pullback:

$$\begin{aligned} \Omega^1_+(M,\mathbb{R}^3) \times \mathrm{Diff}_+(M) &\to \Omega^1_+(M,\mathbb{R}^3) \\ (\alpha,\varphi) &\mapsto \varphi^*\alpha, \end{aligned}$$

where $(\varphi^*\alpha)_x = \alpha_{\varphi(x)} \circ d\varphi_x$. The following proposition summarizes the most important invariances of the metric on $\Omega^1_+(M, \mathbb{R}^3)$:

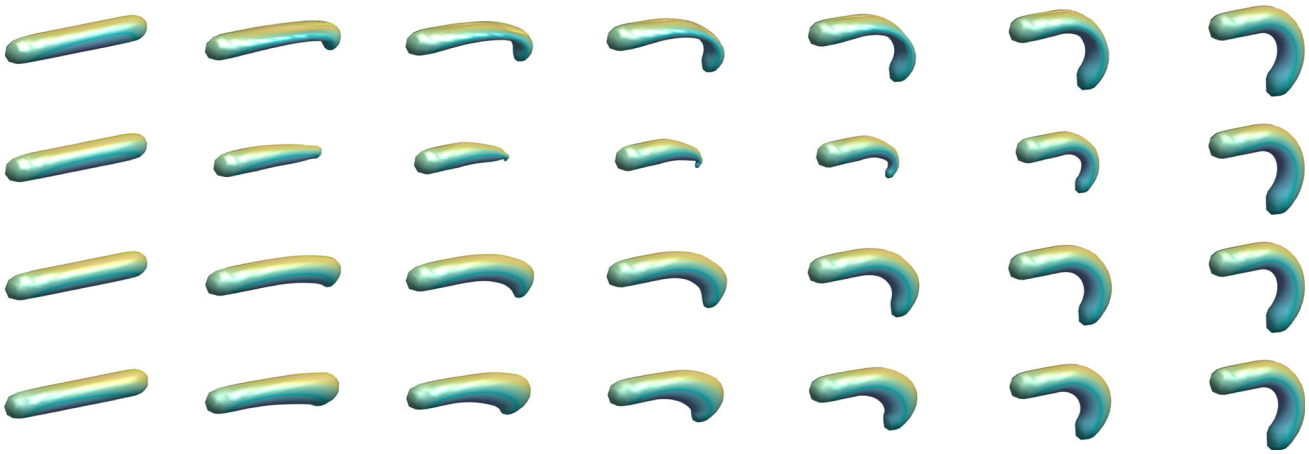

Fig. 3 Geodesics between two cylinders in the space of unparametrized surfaces $\mathrm{Imm}(M,\mathbb{R}^3)/\mathrm{Diff}_+(M)$ with respect to different choices of coefficients (from top to bottom): (1, 1, 0, 1), (1, 0, 1, 1), (1, 1, 1, 0), $(0, \frac{1}{2}, 1, 0)$

Proposition 1 *Let* $\alpha \in \Omega^1_+(M,\mathbb{R}^3)$ *and* $\zeta, \eta \in T_\alpha \Omega^1_+(M,\mathbb{R}^3)$.

1. *Metric* (4) *is invariant under pointwise left multiplication with* SO(3)*, i.e., if* $R \in \mathrm{SO}(3)$*, then*

$$G_\alpha(\zeta,\eta) = G_{R\alpha}(R\zeta, R\eta)$$

2. *Metric* (4) *is invariant under the right action of the diffeomorphism group, i.e., for any* $\varphi \in \mathrm{Diff}_+(M)$*, we have*

$$G_\alpha(\zeta,\eta) = G_{\varphi^*\alpha}(\varphi^*\zeta, \varphi^*\eta).$$

Proof The proof of the proposition follows exactly as for the metric (3), which can be found in [7]. □

The group of rotations SO(3) acts on the space of immersions by left multiplication, which is the same as it acts on the space of one forms. Thus, by the first statement of Proposition 1, the pullback metric on $\mathrm{Imm}(M,\mathbb{R}^3)$ is also invariant under the group of rigid motions $\mathrm{SO}(3) \ltimes \mathbb{R}^3$. For the standard action of $\mathrm{Diff}_+(M)$ by composition from the right on $\mathrm{Imm}(M,\mathbb{R}^3)$, the following commutative diagram illustrates that the pullback action of $\mathrm{Diff}_+(M)$ on $\Omega^1_+(M,\mathbb{R}^3)$ is compatible with the action of $\mathrm{Diff}_+(M)$ on $\mathrm{Imm}(M,\mathbb{R}^3)$:

$$\begin{array}{ccc} f & \xrightarrow{\ d\ } & df \\ \Big\downarrow{\scriptstyle \text{action on } \mathrm{Imm}(M,\mathbb{R}^3)} & & \Big\downarrow{\scriptstyle \text{action on } \Omega^1_+(M,\mathbb{R}^3)} \\ f\circ\varphi & \xrightarrow{\ d\ } & \varphi^* df = df\circ d\varphi \end{array}$$

Therefore, the second statement of Proposition 1 gives the reparametrization invariance of the pullback metric on the space $\mathrm{Imm}(M,\mathbb{R}^3)$.

Thus, the metric on the space of immersions $\mathrm{Imm}(M,\mathbb{R}^3)$ induces a metric on the space of unparametrized surfaces $\mathrm{Imm}(M,\mathbb{R}^3)/\mathrm{Diff}_+(M)$ and a metric on the space of unparametrized surfaces modulo rigid motions $\mathrm{Imm}(M,\mathbb{R}^3)/\left(\mathrm{Diff}_+(M)\times \mathrm{SO}(3)\ltimes\mathbb{R}^3\right)$. In Fig. 3, we show geodesics between two cylinders in the space $\mathrm{Imm}(M,\mathbb{R}^3)/\mathrm{Diff}_+(M)$ with respect to the split metric (4) for different choices of coefficients $\mathfrak{a}$, $\mathfrak{b}$, $\mathfrak{c}$ and $\mathfrak{d}$. The corresponding geodesics in the space $\mathrm{Imm}(M,\mathbb{R}^3)/\left(\mathrm{Diff}_+(M)\times \mathrm{SO}(3)\ltimes\mathbb{R}^3\right)$ are shown in Fig. 4.

3 A Numerical Framework for the General Elastic Metric

In this section, we will describe the discretization and optimization procedure that we implemented to solve the geodesic boundary value problem. From here on, we assume that $M = S^2$ and use a spherical coordinate system to represent an immersion $f : S^2 \to \mathbb{R}^3$ as a function $f : [0, 2\pi] \times [0, \pi] \to \mathbb{R}^3$ such that $f(0,\phi) = f(2\pi,\phi)$, $f(\theta, 0) = f(0, 0)$ and $f(\theta,\pi) = f(0,\pi)$, see Remark 2 below on how we obtain such (discrete) parametrizations in practice from a triangulated surface.

Remark 2 We represent the surface of a given 3D shape with its embedding on a sphere $f : S^2 \to \mathbb{R}^3$, which is always possible for genus-0 surfaces. In practice, methods such as conformal mapping introduce significant distortions when dealing with complex shapes that contain many elongated parts. Since the proposed approach does not require the mapping to be conformal, we adopt the approach of Praun and Hoppe [27], which has been implemented by Kurtek et.al. [24]. The idea is to progressively embed a surface on a sphere while minimizing area distortion. The approach starts by reducing the mesh, using progressive mesh simplification, to a basic polyhedra that can be easily embedded on S^2. Then, it iteratively inserts vertices and embeds each new ver-

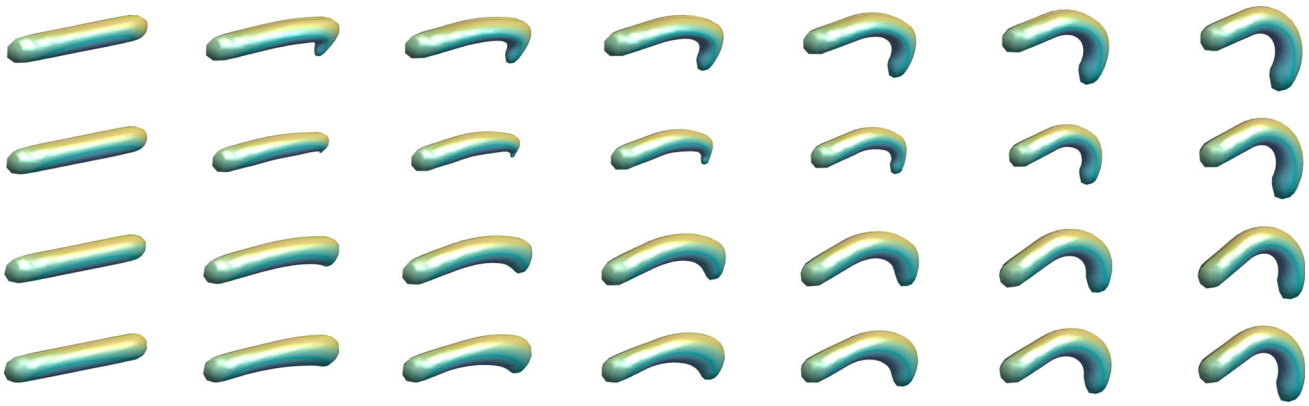

Fig. 4 Geodesics between two cylinders in the space of unparametrized surfaces modulo rigid motions $\mathrm{Imm}(M,\mathbb{R}^3)/\left(\mathrm{Diff}_+(M)\times \mathrm{SO}(3)\ltimes \mathbb{R}^3\right)$ with respect to different choices of coefficients (from top to bottom): $(1,1,0,1)$, $(1,0,1,1)$, $(1,1,1,0)$, $(0,\frac{1}{2},1,0)$. Note that the cylinders in the right are rotated in order to minimize energy beyond what is possible in Fig. 3, which leads to more extensive deformation as well. As compared to Fig. 3, the shapes on the right are rotated by $\theta = 1.54$ and $\phi = 0.21$ (row 1), $\theta = 1.56$ and $\phi = 0.28$ (row 2), $\theta = 1.58$ and $\phi = 0.56$ (row 3) and $\theta = 1.58$ and $\phi = 0.47$ (row 4), where θ and ϕ are the rotation angles around the z-axis and y-axis. All angles are in radians

tex inside the spherical kernel of its one-ring neighborhood while optimizing for the area distortion. Using the implementation provided in [24], we reconstruct the mesh up to 1500 vertices, which is sufficient for computing geodesics. This procedure produces spherical maps that preserve important shape features as shown in all of the examples in this paper. We want to remark here that finding parameterizations of higher genus surfaces is still an open problem. Since we are not aiming at solving the parameterization problem, we focus in this paper on genus-0 manifold surfaces only.

The identity immersion $i : S^2 \to \mathbb{R}^3$ induces the spherical metric on S^2, which will serve as a background metric for the discretization; the vector fields

$$\left\{\frac{1}{\sin\phi}\frac{\partial}{\partial\theta}, \frac{\partial}{\partial\phi}\right\}$$

form an orthonormal basis of the tangent space for any $(\theta,\phi) \in [0,2\pi]\times(0,\pi)$. With respect to this basis and the standard basis on $\mathbb{R}^3$, the differential df of an immersion $f = (x,y,z)^T$ can be represented by a field of 3×2 matrices:

$$df\left(\frac{1}{\sin\phi}\frac{\partial}{\partial\theta}, \frac{\partial}{\partial\phi}\right) = \begin{pmatrix} \frac{1}{\sin\phi}\frac{\partial x}{\partial\theta}, & \frac{\partial x}{\partial\phi} \\ \frac{1}{\sin\phi}\frac{\partial y}{\partial\theta}, & \frac{\partial y}{\partial\phi} \\ \frac{1}{\sin\phi}\frac{\partial z}{\partial\theta}, & \frac{\partial z}{\partial\phi} \end{pmatrix}.$$

In the following, we denote by $\|\cdot\|_f$ the norm induced by the pullback of the split metric (4) and let $u \in T_f\,\mathrm{Imm}(S^2,\mathbb{R}^3)$ be a tangent vector. Since u can be seen as a function from S^2 to $\mathbb{R}^3$, using this representation, the norm of u with respect to the split metric will be given as follows:

$$\|u\|_f = \left[G_{df}^{\mathfrak{a},\mathfrak{b},\mathfrak{c},\mathfrak{d}}(du,du)\right]^{1/2}.$$

3.1 Geodesics in the Space of Surfaces

We will now describe the solution of the boundary value problem in the preshape space of all parametrized surfaces.

Remark 3 We should emphasize here that the space of immersions with respect to the proposed family of Riemannian metrics is not geodesically convex. Thus, the solution of the minimization problem might not exist in the space of immersions but only in a larger space of functions (including those with possibly degenerate differential). In fact, for $\dim M \geq 2$, there exists no Riemannian metric on the space of immersions for which geodesic completeness or convexity results have been obtained; in the case of immersed curves, such results have been achieved for metrics of order two or higher [9], but it remains unknown for our higher dimensional situation.

Given two parametrized surfaces f_1 and f_2, we can discretize the linear path connecting f_1 and f_2 in T time steps:

$$f_{\mathrm{lin}}(t_i) = (1-t_i)f_1 + t_i f_2.$$

where $t_i = i/T$, $i = 0,\ldots,T$. The differential df_{lin} is then the linear path between df_1 and df_2, which stays by definition in the space of exact one-forms for all $i = 0,\ldots,T$. Note that this path does not necessarily stay in the space of full-ranked one-forms, e.g., if $df_1 = -df_2$ for some $x \in S^2$. However,

we did not encounter any problems with this possible degeneracy. To solve the geodesic boundary value problem, we will perturb $f(t)$ in all possible directions that fix the end points and that remain in the space of immersions. Since the map d, as defined in Equation (2), is injective, this is equivalent to perturbing the differential $df(t)$ in all possible directions in the space of exact one-forms that keep the two boundary one-forms fixed.

To obtain a basis of perturbations in the space of immersions, we use the fact that the set of spherical harmonics in each component form a Hilbert basis of $L^2(S^2, \mathbb{R}^3)$. We truncate this basis at a chosen maximal degree deg and denote the obtained set by $\{S_i\}$. The number of elements in this basis is $L = 3((\deg+1)^2 - 1)$ (here, we remove the spherical harmonic of degree 0 and order 0 since it is a constant function, which corresponds to a pure translation). To calculate the optimal deformation between two given surfaces, we aim to minimize the (discrete) path energy over all curves of the form

$$f(t_0) = f_1, \quad f(t_T) = f_2$$
$$f(t_i) = (1-t_i)f_1 + t_i f_2 + \sum_{j=1}^{L} \mathrm{Coeff}(j,i) S_j, \tag{5}$$

where $i = 1, \ldots, T-1$ and Coeff is a $L \times (T-1)$ coefficient matrix.

The discrete energy functional $F : \mathbb{R}^{L\times(T-1)} \to \mathbb{R}$ is then given by

$$F(\mathrm{Coeff}) = \sum_{i=1}^{T} \| f_t(t_{i-1}) \|^2_{f(t_{i-1})} \, \Delta T \tag{6}$$

where the norm $\|\cdot\|$ is induced by the pullback of the split metric (4),

$$f_t(t_{i-1}) = \frac{f(t_i) - f(t_{i-1})}{\Delta T} \tag{7}$$

is the (discrete) derivative of $f(t)$ at $f(t_{i-1})$ and $\Delta T = \frac{1}{T}$ is the width of a subinterval. Alternatively, one can also discretize the derivative of f using the central difference for interior data points, which makes the energy functional symmetric, but leads to slightly higher computational cost. To find the optimal coefficient matrix Coeff, we employ a BFGS method, which is a quasi-Newton method for solving unconstrained minimization problems [13], as provided in the optimize package of *scipy*. We calculate the gradient using automatic differentiation in *Pytorch*, which leads to the algorithm described in Algorithm 1. See [21] for more examples of applying tools of deep learning and in particular automatic differentiation in shape and image analysis.

Algorithm 1 The matching problem for parametrized surfaces

Input:

1) the source and target surfaces f_1 and f_2;
2) the coefficients $(\mathfrak{a}, \mathfrak{b}, \mathfrak{c}, \mathfrak{d})$ of the metric;
3) the number of time steps T;
4) a basis $\{S_i, i = 1, \ldots, L\}$ for the space of parametrized surfaces.

Output:

1) the geodesic f_{geo} connecting f_1 to f_2;
2) the geodesic distance dist between f_1, and f_2;

1: Initialize Coeff $= 0$ and $f(t_i)$ by equation (5).
2: Compute $f_t(t_{i-1})$ by equation (7).
3: Define the functional F(Coeff) as in equation (6).
4: Minimize F using a BGFS-method, where the gradient of F with respect to Coeff is calculated using the automatic differentiation package in Pytorch.
5: Set

$$f_{\mathrm{geo}}(t_0) = f_1, \qquad f_{\mathrm{geo}}(t_T) = f_2$$
$$f_{\mathrm{geo}}(t_i) = (1-t_i)f_1 + t_i f_2 + \sum_{j=1}^{L} \mathrm{Coeff}(j,i) S_j$$

and dist $= \sqrt{F(\mathrm{Coeff})}$.
6: **return** f_{geo} and dist.

3.2 Geodesics in the Space of Unparametrized Surfaces

Now we present our algorithm for calculating geodesics in the space of unparametrized surfaces $\mathrm{Imm}(S^2, \mathbb{R}^3)/\mathrm{Diff}_+(S^2)$. The main difficulty for this task is to find the optimal $\gamma \in \mathrm{Diff}_+(S^2)$ that realizes the distance

$$\mathrm{dist}_{\mathcal{S}}([f_1],[f_2]) = \inf_{\gamma\in\mathrm{Diff}_+(S^2)} \mathrm{dist}_{\mathrm{Imm}}(f_1\circ\gamma, f_2),$$

where $[f]$ is the equivalence class of f under the action of the group of orientation-preserving diffeomorphisms $\mathrm{Diff}_+(S^2)$ and $\mathrm{dist}_{\mathcal{S}}$ denotes the distance function on the space $\mathrm{Imm}(S^2, \mathbb{R}^3)/\mathrm{Diff}_+(S^2)$ with respect to the metric that is induced from the split metric (4).

In order to practically perform the minimization over the infinite-dimensional space $\mathrm{Diff}_+(S^2)$, we have to choose a suitable discretization of this group: Let Id be the identity map from S^2 to itself. The tangent space $T_{\mathrm{Id}}\,\mathrm{Diff}_+(S^2)$ is the set of all (smooth) vector fields on S^2. The set of gradient and skew gradient vector fields of the set of spherical harmonics provides an orthogonal basis for this tangent space—here orthogonal means with respect to the standard L^2 metric, see, e.g., [22]. Normalizing these basis, we obtain an orthonormal basis for the tangent space $T_{\mathrm{Id}}\,\mathrm{Diff}_+(S^2)$. To choose a finite-dimensional discretization of the tangent space, we truncate this basis at a maximal degree $\overline{\deg}$; then, the number of elements in this basis is $\bar{L} = 2(\overline{\deg}+1)^2 - 2$. From here on,

we will denote this truncated basis by $\{v_i, i = 1, ..., \bar{L}\}$. Let $X^v = (X_1^v, X_2^v, \ldots, X_{\bar{L}}^v)$ be the coefficients of a vector field with respect to this basis, and consider the induced mapping

$$\gamma = \text{Proj}\left(\text{Id} + \sum_{k=1}^{\bar{L}} X_k^v v_k\right), \tag{8}$$

where $\text{Proj}(x) = \frac{x}{|x|}$ denotes the map that projects nonzero vectors in $\mathbb{R}^3$ onto the unit sphere $S^2 \subset \mathbb{R}^3$. The following result gives an explicit bound on the size of X^v that ensures that the corresponding γ, defined by (8), is a diffeomorphisms of S^2.

Theorem 3 *Let $U = \sum_{k=1}^{\bar{L}} X_k^v v_k$ be a vector field on the sphere S^2 and let $\gamma = \text{Proj}\,(\text{Id} + tU)$ be the corresponding map as defined in (8), for some real t. Then, γ is a diffeomorphism if*

$$|t| < -\frac{1}{\inf_{p\in M} \lambda_-(\nabla U)}, \tag{9}$$

where ∇U is the $(1, 1)$ tensor field $v \mapsto \nabla_v U$ and $\lambda_-(\nabla U)$ is the smaller of the two real eigenvalues of the symmetrized matrix $\overline{\nabla U} = \frac{1}{2}\big(\nabla U + (\nabla U)^T\big)$.

Note that ∇U is a tensor that for each point $x \in S^2$ gives a linear transformation $T_x S^2 \to T_x S^2$, which is defined by $\nabla U(v)$ being the covariant derivative of U in the direction v.

Proof The proof of this result is postponed to "Appendix B." Note that since $\text{Tr}(\nabla U) = \text{div} U$, which integrates to zero over the compact manifold M, we know that $\lambda_-(\nabla U)$ is always negative somewhere; hence, the bound on $|t|$ is some positive number. □

We are now able to describe the discrete optimization problem on the space of unparametrized surfaces, i.e., we aim to minimize the discrete functional $\bar{F} : \mathbb{R}^{\bar{L}+L\times(T-2)} \to \mathbb{R}$ given by

$$\bar{F}(X^v, \text{Coeff}) = \sum_{i=1}^{T} \|f_t(t_{i-1})\|^2_{f(t_{i-1})}\, \Delta T, \tag{10}$$

where the norm $\|\cdot\|$ is induced by the pullback of the split metric (4), Coeff, S_i, $\Delta T = \frac{1}{T}$ are as in Sect. 3.1 and where the discrete curve f is now of the form

$$f(t_0) = f_1 \circ \gamma, \quad f(t_T) = f_2$$
$$f(t_i) = (1 - t_i) f_1 + t_i f_2 + \sum_{j=1}^{L} \text{Coeff}(j, i) S_j, \tag{11}$$

and where the reparametrization γ is given by formula (8) with coefficient vector $X^v = (X_1^v, X_2^v, \ldots, X_{\bar{L}}^v)$.

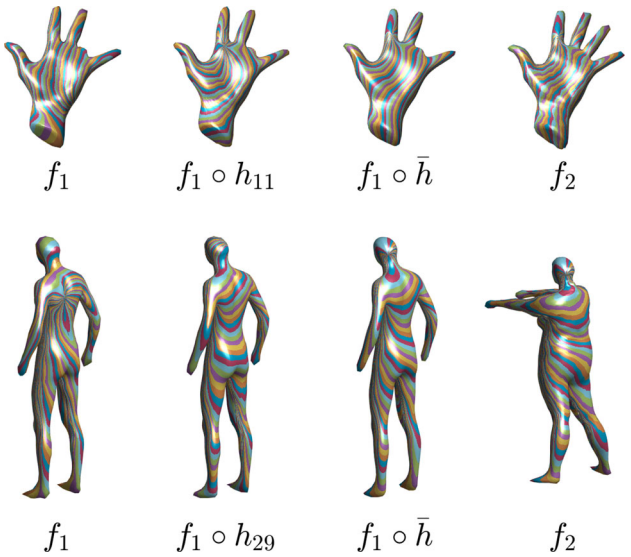

Fig. 5 Examples of boundary surfaces before and after the optimization over the reparametrization group with respect to the split $(1, 1, 1, 0)$ metric. Here, the second shape shows the parametrization of the first boundary surface after composing by the initial guess in the icosahedral group and the third shape shows the final point correspondences after the full optimization, where $\bar{h}$ denotes the optimal reparametrization. One can observe how the parametrization of the initial surface successively better matches the parametrization of the target surface (the color map represents the parametrization of the surfaces)

Remark 4 (*Initialization over* $\text{Diff}_+(S^2)$) When using a gradient-based optimization method, it is always an important issue to find a good initialization, as the optimization procedure can get stuck in local minima and is usually sensitive to this initialization. In order to find a good initial guess for the optimal reparametrization of the surface f_1, we first align the corresponding SRNFs of the two boundary surfaces f_1 and f_2. This seems a natural initialization for the $(0, \frac{1}{2}, 1, 0)$ metric as the L^2-distance on the space of SRNFs is a first-order approximation of the geodesic distance of this metrics. However, in all our experiments, it turned out that this initialization works well for other choices of constants as well, as the optimal point correspondences for different choices of constants, albeit different, are still similar on a global scale. Furthermore, we note that any three-dimensional rotation can be seen as a diffeomorphism of S^2. We use this fact to first minimize only over this finite-dimensional subgroup of the infinite-dimensional reparametrization group. Finally, to initialize the optimization over this finite-dimensional group, we first consider the icosahedral group, which contains 60 orientation-preserving rotations denoted by $h_i, i = 1, \ldots, 60$, as a finite subset of SO(3). We then choose the best diffeomorphism among these 60 elements as our initial guess. See Fig. 5 for examples of registration before and after this initialization and the whole optimization process over the group of orientation-preserving diffeomorphisms $\text{Diff}_+(S^2)$.

In the following, we will describe two algorithms for calculating geodesics in the space of unparametrized surfaces $\mathrm{Imm}(S^2, \mathbb{R}^3)$: a *joint optimization* procedure and a *coordinate descent* approach, where we minimize alternating in the space of parametrized surfaces and over the reparametrization group separately.

We will start by describing the joint optimization procedure, which is analogous to the optimization for parametrized surfaces with one caveat: Since Formula (8) only leads to diffeomorphisms near the identity, i.e., reparametrizations that map points on S^2 to nearby points, we will describe large deformations between S^2 as a composition of N such (small) deformations. This will lead us to iteratively solve the joint optimization problem. The corresponding algorithm is described in Algorithm 2.

Algorithm 2 The joint optimization approach

Input:

1) the source and target surfaces f_1 and f_2;
2) the coefficients $(\mathfrak{a}, \mathfrak{b}, \mathfrak{c}, \mathfrak{d})$ of the metric;
3) the number of time steps T;
4) bases $\{S_i, i = 1, \dots, L\}$ and $\{v_i, i = 1, \dots, \tilde{L}\}$ for the space of parametrized surfaces and vector fields on S^2 resp.;
5) the number N that describes the maximal amount of small deformations used.

Output:

1) the geodesic f_{geo} connecting $[f_1]$ to $[f_2]$;
2) the geodesic distance dist between $[f_1]$ and $[f_2]$;

1: Initialize $\bar{f} = f_1$, Coeff $= 0$
2: **while** $k \leq N$ **do**
3: Initialize γ by Formula (8) with $X^v = 0$ and $f(t_i)$ by Equation (11).
4: Compute $f_t(t_{i-1})$ by Equation (7).
5: Define the functional $\bar{F}(X^v, \mathrm{Coeff})$ by (10) where the discrete curve f is of the form

$$f(t_0) = \bar{f} \circ \gamma, \quad f(t_T) = f_2$$

$$f(t_i) = (1 - t_i) f_1 + t_i f_2 + \sum_{j=1}^{L} \mathrm{Coeff}(j, i) S_j,$$

6: Minimize $\bar{F}$ using a BFGS method, where the gradients of $\bar{F}$ with respect to X^v and Coeff are calculated using the automatic differentiation package in Pytorch.
7: Compute the optimal γ using Formula (8).
8: Update $\bar{f} = \bar{f} \circ \gamma$.
9: $k = k + 1$
10: **end while**
11: Set

$$f_{\mathrm{geo}}(t_0) = \bar{f}, \qquad f_{\mathrm{geo}}(t_T) = f_2$$

$$f_{\mathrm{geo}}(t_i) = (1 - t_i) f_1 + t_i f_2 + \sum_{j=1}^{L} \mathrm{Coeff}(j, i) S_j,$$

and dist $= \sqrt{\bar{F}(X^v, \mathrm{Coeff})}$.
12: **return** f_{geo} and dist

As an alternative to the joint optimization, we will present in the following a *coordinate descent method*, where we separate the variables in the space of surfaces from the variables that govern the reparametrization of the initial surface, i.e., we alternate between calculating a discrete geodesic, denoted by f_{opt}, between the parametrized surfaces f_1 and f_2 in the space of immersions $\mathrm{Imm}(S^2, \mathbb{R}^3)$ and reparametrizing the initial surface $\bar{f} = f_1$. To update the reparametrization, we consider only the first two time points of f_{opt}, i.e., $\bar{f}$ and $f_{\mathrm{opt}}(t_1)$ and define the following functional

$$F_r(X^v) = \left\| f_{\mathrm{opt}}(t_1) - \bar{f} \circ \gamma \right\|^2_{\bar{f} \circ \gamma}, \tag{12}$$

where γ is given by Formula (8) and $X^v = (X_1^v, X_2^v, \dots, X_{\tilde{L}}^v)$. We can now employ a BFGS method to find the optimal coefficient vector X^v_{opt}, compute γ using Formula (8) and then update $\bar{f} = \bar{f} \circ \gamma$. Then, we repeat this process by recalculating the geodesic in the space of parametrized surfaces (with the changed initial surface $\bar{f}$). The whole optimization process is summarized in Algorithm 3.

3.3 Geodesics in the Space of Unparametrized Surfaces Modulo Rigid Motions

Note that the split metric (4) associates no cost with translation and thus the obtained geodesic is automatically in the space of surfaces modulo translations. To calculate the geodesic between two surfaces $[f_1]$ and $[f_2]$ in the space of unparametrized surfaces modulo rigid motions $\mathrm{Imm}(S^2, \mathbb{R}^3) / \left(\mathrm{Diff}_+(S^2) \times \mathrm{SO}(3) \ltimes \mathbb{R}^3\right)$, we will need to minimize in addition over the rotation group, i.e., solve the optimization problem on $\mathrm{SO}(3) \times \mathrm{Diff}_+(S^2)$:

$$\mathrm{dist}_{\mathcal{S}}([f_1], [f_2]) = \inf_{\substack{R \in \mathrm{SO}(3) \\ \gamma \in \mathrm{Diff}_+(S^2)}} \mathrm{dist}_{\mathrm{Imm}}(f_1 \circ \gamma, R f_2),$$

where $[f]$ is the equivalence class of f under the actions of $\mathrm{Diff}_+(S^2)$ and $\mathrm{SO}(3)$ and $\mathrm{dist}_{\mathcal{S}}$ denotes the distance function on the space $\mathrm{Imm}(S^2, \mathbb{R}^3) / \left(\mathrm{Diff}_+(S^2) \times \mathrm{SO}(3) \ltimes \mathbb{R}^3\right)$.

Let $\|\cdot\|$, Coeff, S_i, ΔT be as in Sect. 3.1, and let $\bar{f}$ be the current parametrization of the first boundary surface. It is known that the group of rotations $\mathrm{SO}(3)$ is a three-dimensional Lie group and the matrix exponential exp from its Lie algebra $\mathfrak{so}(3)$ is surjective. Since there is an isomorphism between $\mathbb{R}^3$ and $\mathfrak{so}(3)$, the discrete optimization problem on the space of unparametrized surfaces modulo rigid motions will be minimizing the discrete functional $\tilde{F} : \mathbb{R}^{3+\tilde{L}+L\times(T-2)} \to \mathbb{R}$ given by

$$\tilde{F}(X^R, X^v, \mathrm{Coeff}) = \sum_{i=1}^{T} \| f_t(t_{i-1}) \|^2_{f_{i-1}} \Delta T,$$

where the discrete curve in this case is of the form

Algorithm 3 The coordinate descent approach

Input:

1) the source and target surfaces f_1 and f_2;
2) the coefficients $(\mathfrak{a}, \mathfrak{b}, \mathfrak{c}, \mathfrak{d})$ of the metric;
3) the number of time steps T;
4) bases $\{S_i, i = 1, \ldots, L\}$ and $\{v_i, i = 1, \ldots, \bar{L}\}$ for the space of parametrized surfaces and vector fields on S^2 resp;
5) the number N that describes the maximal amount of small deformations used.

Output:

1) the geodesic f_{geo} connecting $[f_1]$ to $[f_2]$;
2) the geodesic distance dist between $[f_1]$ and $[f_2]$;

Let $\bar{f} = f_1$ and initialize Coeff $= 0$.
Choose a positive integer N.
while $k \leq N$ **do**
  Define the functional $F(\text{Coeff})$ by (6) where the discrete curve f is of the form

$$f(t_0) = \bar{f}, \quad f(t_T) = f_2$$
$$f(t_i) = (1 - t_i) f_1 + t_i f_2 + \sum_{j=1}^{L} \text{Coeff}(j, i) S_j,$$

  Minimize $F(\text{Coeff})$ using a BFGS method, where the gradient of F with respect to Coeff is calculated using the automatic differentiation package in Pytorch.
  Calculate $f_{\text{opt}}(t_1) = \sum_{i=1}^{L} \text{Coeff}(i, 1) S_i$.
  Initialize $X^v = 0$ and γ by Formula (8).
  Define the functional $F_r(X^v)$ by Equation (12).
  Minimize F_r using a BFGS method with gradient of F_r with respect to X^v calculated using the automatic differentiation package.
  Compute γ using Formula (8).
  Update $\bar{f} = \bar{f} \circ \gamma$.
  $k = k + 1$
end while
Set

$$f_{\text{geo}}(t_0) = \bar{f}, \quad f_{\text{geo}}(t_T) = f_2$$
$$f_{\text{geo}}(t_i) = (1 - t_i) f_1 + t_i f_2 + \sum_{j=1}^{L} \text{Coeff}(j, i) S_j,$$

and dist $= \sqrt{F(\text{Coeff})}$.
return f_{geo} and dist

$$f(t_0) = \bar{f} \circ \gamma, \quad f(t_T) = \exp(X^R) f_2$$
$$f(t_i) = (1 - t_i) f_1 + t_i f(t_T) + \sum_{j=1}^{L} \text{Coeff}(j, i) S_j,$$

$i = 1, \cdots, T - 1$ and where the reparametrization γ is given by Formula (8) with coefficient vector $X^v = (X_1^v, X_2^v, \ldots, X_{\bar{L}}^v)$. We will tackle this simpler (finite-dimensional) optimization problem using an analogous approach as in the previous section and will thus omit further details (Fig. 6).

4 Experiments

In this section, we will present examples of geodesics as calculated using our optimization procedures. The human body shapes have been kindly provided by Nil Hasler [15], and the hand shape is taken from SHREC07 watertight models. All other shapes are courtesy of the TOSCA shape database [8].

4.1 Geodesics and Karcher Mean

In Fig. 8, we present examples of geodesics between given surfaces in the space $\text{Imm}(S^2, \mathbb{R}^3)/\text{Diff}_+(S^2)$ with respect to the split $(1, 1, 0.1, 0)$ metric and the corresponding evolutions of energies. In all our examples, we observed a good and relatively fast convergence of the optimization procedure, and we present some selected results of the resulting deformation and the corresponding computation times in Table 1. In Fig. 7, we present the Karcher mean of a family of cat surfaces with respect to the split $(1, 1, 0.1, 0)$ metric in the space of unparametrized surfaces modulo rigid motions $\text{Imm}(S^2, \mathbb{R}^3)/(\text{Diff}_+(S^2) \times \text{SO}(3) \ltimes \mathbb{R}^3)$. One can observe that the mean captures the overall characteristics of the family of surfaces under consideration, but simplifies some of the features that undergo high variability. To calculate the Karcher mean, we followed an iterative algorithm as described e.g. in [12] in the context of diffeomorphism-based shape analysis. In this method, one arbitrarily orders the data points as $f_1, \ldots, f_n$ and let q_1 be the midpoint of the geodesic between f_1 and f_2. Then, one defines q_{i+1} by travelling until time $\frac{1}{i+1}$ on the geodesic that connects q_{i-1} to f_{i+1} in time 1. The approximation of the Karcher mean is then given by q_{n-1}. We want to remark here that this method depends on the ordering of the data points (initialization), and in future work, we plan to further investigate this and compare it to other Karcher mean algorithms, such as directly minimizing the sum of squares of geodesic distances. All results were obtained on a standard laptop without any parallelization or GPU implementation, which could certainly be used to obtain a significant increase in speed (Fig. 8).

Remark 5 The results in Table 1 suggest that our methods are well suited for multiresolution methods, i.e., to solve the geodesic matching problem first on a coarser resolution (in time, space and degree of spherical harmonics) and then use an upsampled version of the previously obtained solution as initial guess for solving a high-resolution version of the matching problem. Our numerical framework allows for these approaches in all available parameters, and in all our experiments, this procedure seems to allow for as moderate improvements in the speed of the optimization. See Fig. 6 for an example of a multiresolution geodesic in spatial resolution.

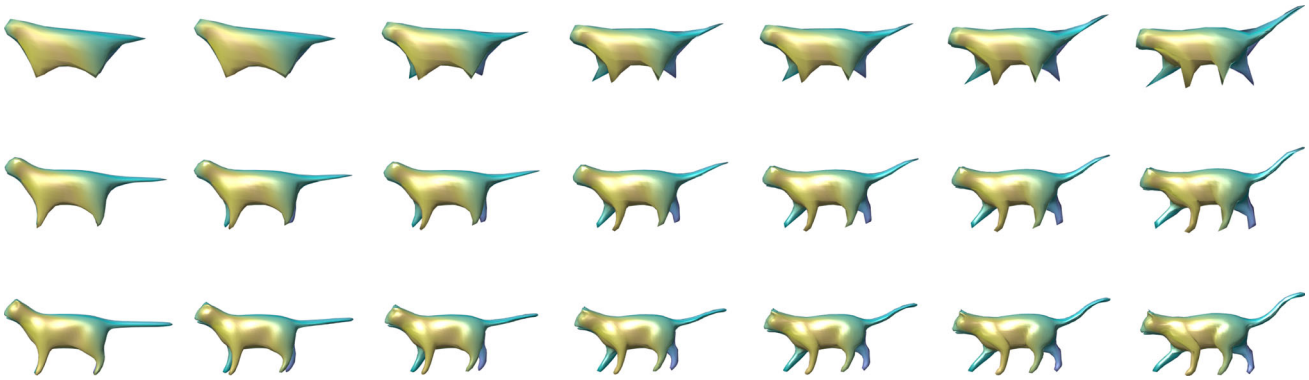

Fig. 6 Example of a geodesic in several resolutions: 12×25 (top), 25×49 (middle) and 50×99 (bottom) with respect to the split $(1, 1, 0.1, 0)$ metric in the space of unparametrized surfaces $\mathrm{Imm}(S^2, \mathbb{R}^3)/\mathrm{Diff}_+(S^2)$, where $\mathrm{deg} = 7$, $\overline{\mathrm{deg}} = 7$ and $T = 13$

Table 1 Numerical results of matching surfaces with different resolutions in time and space: low: 12×25, $\mathrm{deg} = \overline{\mathrm{deg}} = 5$, $T = 5$; middle: 25×49, $\mathrm{deg} = 7$, $\overline{\mathrm{deg}} = 8$, $T = 10$; and high: 50×99, $\mathrm{deg} = 9$, $\overline{\mathrm{deg}} = 11$, $T = 15$. Here, Iter denotes the number of iterations until convergence in the optimization process

Boundary Surfaces	Resolution	Iter	RunTime
	low	114	39.7s
	middle	237	3min 3s
	high	235	14min 2s
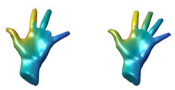	low	42	40.7s
	middle	113	1min 35s
	high	139	8min 25s
	low	88	32.5s
	middle	220	2min 22s
	high	193	10min 27s

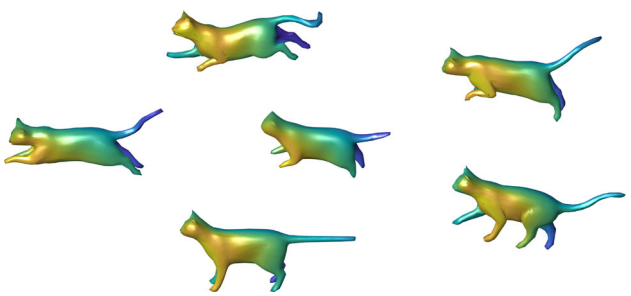

Fig. 7 Karcher mean (middle) of a set of shapes of cats in the space $\mathrm{Imm}(S^2, \mathbb{R}^3)/(\mathrm{Diff}_+(S^2) \times \mathrm{SO}(3) \ltimes \mathbb{R}^3)$ with respect to the split $(1, 1, 0.1, 0)$ metric

4.2 Comparison to the SRNF Framework

Finally, we aim to compare the results obtained with our method to the results using the inversion of linear paths in the SRNF space. The SRNF metric corresponds to the split metric (4) with constant $(0, 1/2, 1, 0)$, see "Appendix B." To demonstrate this correspondence, we consider four pairs of boundary surfaces. We calculated the length of the linear path between each pair of surfaces under the split $(0, 1/2, 1, 0)$ and the length of the image of the linear path under the SRNF framework. The relative errors between the lengths for different time step sizes are shown in Table 2 and demonstrate that these two metrics indeed coincide.

Since the image of the SRNF map is not convex in L^2, the linear interpolation between two SRNFs may not have a preimage under the SRNF map. Also, even for functions that are in the image of SRNF map, the inverse does not have an analytic expression; in fact, such an expression does not exist in general, since the SRNF map is not injective. As a way to overcome this difficulty, Laga et al. [25] introduced a numerical method to calculate an approximated inversion of any path between two given SRNFs. In practice, this has been used to approximate the geodesic by inverting the linear path between the given SRNFs. We want to remark here that the algorithm of [25] could also be used to invert a geodesic in the image of the SRNF map. However, calculating geodesics in the image of the SRNF map is a nontrivial process, which to the best of our knowledge has not yet been attempted. We would expect that this procedure would lead to minimizers that recover the minimizers obtained in the present framework. In Fig. 9, we consider two pairs of surfaces and calculate the geodesic between each pair of the boundary surfaces under the split $(0, 1/2, 1, 0)$ metric with $\mathrm{deg} = \overline{\mathrm{deg}} = 7$, $T = 13$ in the space of unparametrized surfaces $\mathrm{Imm}(S^2, \mathbb{R}^3)/\mathrm{Diff}_+(S^2)$. The comparisons of these geodesics with the approximated inversions of the linear paths between the boundary surfaces are shown in Fig. 9. One can see that in the last row for the geodesic between the human body surfaces, the arms are shrinking at the beginning and then stretching, which may be not a desired deformation for some applications. However, by adjusting the coefficients of our metric, we could obtain geodesics with the natural

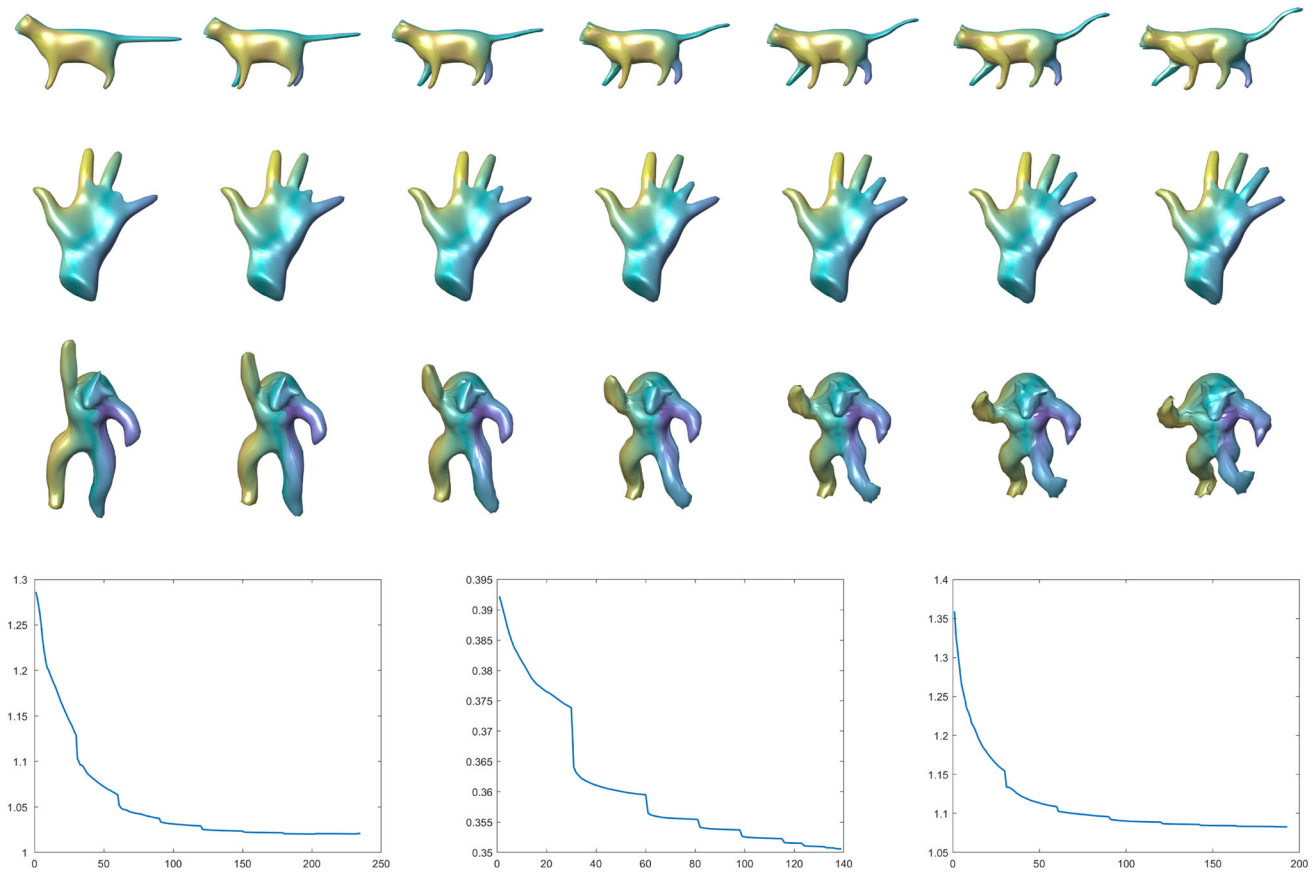

Fig. 8 Examples of geodesics w.r.t. to the $(1, 1, 0.1, 0)$ metric in the space of shapes $\mathrm{Imm}(S^2, \mathbb{R}^3)/\mathrm{Diff}_+(S^2)$, where we choose a resolution of 50×99, a maximal degree of spherical harmonics $\mathrm{deg} = \overline{\mathrm{deg}} = 7$ and 13 timesteps, i.e., we search in an approximately 2205-dimensional space. The corresponding energy evolution for each example is shown on the bottom from left to right

Table 2 Comparisons between the lengths of linear paths with respect to the split $(0, \frac{1}{2}, 1, 0)$ metric and the lengths of the SRNF representations of the linear paths with respect to the L^2 metric. L_l: the length of linear path; L_{L_2}: the length of the SRNF representation of the linear path with respect to the L^2 metric

Boundary Surfaces	Tstps	L_l	L_{L^2}	Relative Error
	13	0.8917	0.8872	0.00502
	20	0.8952	0.8908	0.00494
	99	0.8952	0.8952	0.00002
	13	0.7384	0.7350	0.00456
	20	0.7372	0.7359	0.00169
	99	0.7371	0.7367	0.00053
	13	0.6722	0.6717	0.00072
	20	0.6722	0.6720	0.00030
	99	0.6723	0.6723	0.00002
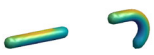	13	0.9875	0.9853	0.00226
	20	0.9874	0.9866	0.00084
	99	0.9875	0.9875	0.00004

behavior, see Fig. 10 for geodesics with respect to different choices of coefficients.

In Table 3, we compare the lengths of geodesics for four pairs of surfaces in the space of parametrized surfaces $\mathrm{Imm}(S^2, \mathbb{R}^3)$, the lengths of the approximated inversions (with seven time steps) under the split $(0, 1/2, 1, 0)$ metric and the L^2 differences between the SRNFs of the boundary surfaces. One can see from the table that for each pair of surfaces, the length of the geodesic is much closer to the L^2 difference than the length of the approximated inversion of the straight line between the SRNFs of the boundary surfaces. Note that the L^2-difference is a lower bound for the geodesic distance that will, in general, be strictly smaller than the true geodesic distance, as the image of the SNRF-representation is not a totally geodesic (open) subspace of the space of all L^2-functions.

Fig. 9 Comparisons of geodesics with respect to the split $(0, \frac{1}{2}, 1, 0)$ metric and the approximated inversions of straight lines under the SRNF framework. Row 1, 3: the approximated inversions under the SRNF framework; Row 2, 4: geodesics under the split $(0, \frac{1}{2}, 1, 0)$ metric in the space of parametrized surfaces

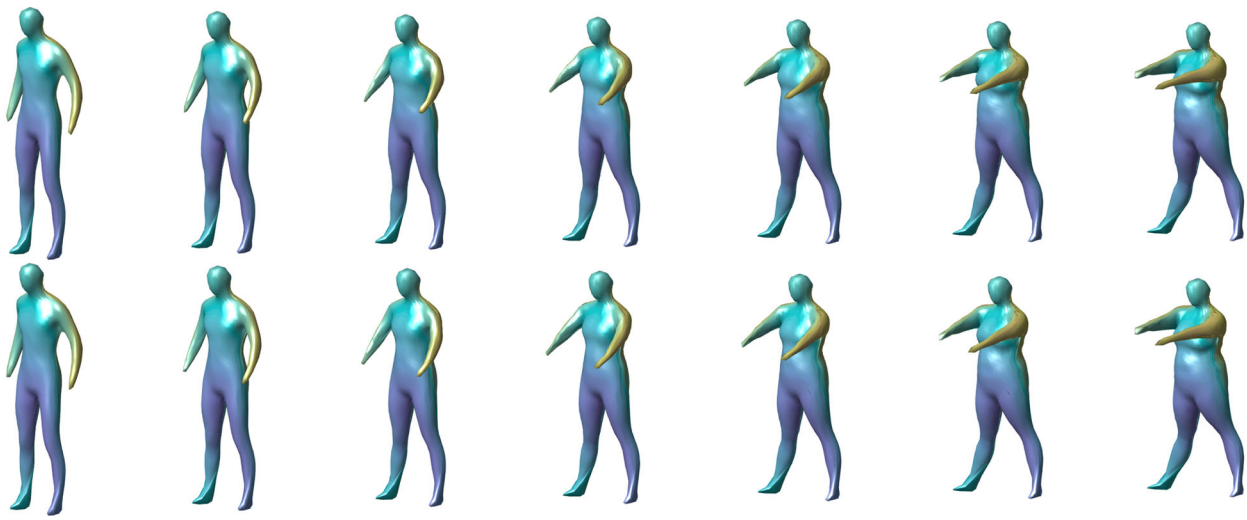

Fig. 10 Geodesics between two human body surfaces in the space of unparametrized surfaces $\mathrm{Imm}(S^2, \mathbb{R}^3)/\operatorname{Diff}_+(S^2)$ with respect to two different choices of coefficients $(0, 1, 1, 0)$ (top) and $(1, 1, 0.1, 0)$ (bottom). In particular, in the deformation of the arms, one can observe the influence of the constants

5 Conclusion

In this article, we have introduced a family of elastic metrics on the space of parametrized surfaces in 3D space using a corresponding family of metrics on the space of vector-valued one-forms. For this class of metrics, we have provided a numerical framework for the computation of geodesics on the space of both parametrized and unparametrized surfaces. This new class of metrics generalizes a previously studied family of elastic metrics and includes, in particular, the Square Root Normal Field (SRNF) metric, which has been proven successful in various applications. In the numerical experiment, provided in Sect. 4, we have demonstrated our framework by showing several examples of geodesics

Table 3 Lengths of deformations with respect to the $(0, \frac{1}{2}, 1, 0)$ metric between boundary surfaces with the maximal spherical harmonic degree of 7 and time step size of 25. L_l: the length of the linear path between boundary surfaces; L_g: the length of geodesic as calculated in our numerical framework; L_i: the length of approximated inversion from SRNF straight line; and L^2-Diff: the L^2 difference between the SRNFs of these boundary surfaces

Boundary Surfaces	L_l	L_g	L_i(7stps)	L^2 Diff
	0.8932	0.7948	1.1442	0.6130
	0.7380	0.7171	0.7919	0.6543
	0.6723	0.5985	0.8393	0.5938
	0.9875	0.7973	1.2159	0.7786

and compared our results with earlier results obtained from the SRNF framework. Our framework does not require a numerical inversion of the SRNF map and thus overcomes some of the difficulties of previous work. Furthermore, it allows to choose the constants of the metric in a data-driven way, which has potential importance in many applications. In future work, we plan to further demonstrate the viability of the proposed method in applications to real data. In addition, we are currently working toward developing a generalization of the SRNF map that will allow us to approximate the geodesic distance for our general class of metrics and will thus speed up the computation by choosing a better initial guess for the parametrization of the boundary surface.

Acknowledgements The authors thank Anuj Srivastava and all the members of the Florida State statistical shape analysis group for helpful discussions during the preparation of this manuscript. In addition, we are grateful to Sebastian Kurtek and Alice Barbara Tumpach for discussion about the implementation of the minimization over the diffeomorphism group.

Appendix A: The Geodesic Equation

In the following, we give the geodesic equation on the space of immersions $\mathrm{Imm}(M, \mathbb{R}^3)$ with respect to the pullback of the metric (3) on the space of 1-forms. In this "Appendix," we will assume that the domain M is a compact orientable surface without boundary, because we will need to use the Hodge decomposition. We will view $\alpha \in \Omega^1_+(M, \mathbb{R}^3)$ as a vector-valued 1-form with components $(\alpha^1, \alpha^2, \alpha^3)$, where each α^i is a 1-form on M in the usual sense. Then, metric (3) can be rewritten as

$$G_\alpha(\xi, \xi) = \int_M \mathrm{tr}(\xi\, \Lambda_\alpha \xi^T)\, \varphi_\alpha\, \mu = \sum_{i=1}^{3} \int_M \langle \xi^i_x,\, \Lambda_\alpha \xi^i_x \rangle\, \varphi_\alpha\, \mu$$

where $\xi = (\xi^1, \xi^2, \xi^3) \in T_\alpha \Omega^1_+(M, \mathbb{R}^3)$, $\Lambda_\alpha = (\alpha^T \alpha)^{-1}$ is the induced Riemannian metric on 1-forms on M, and $\varphi_\alpha = \sqrt{\det(\alpha^T \alpha)}$ is the induced volume form on M. As such, all computations can be done one component at a time.

If $F = (f^1, f^2, f^3)$ is a vector-valued function with each $f^i : M \to \mathbb{R}$ real-valued, then $\beta = dF$ is a vector-valued 1-form with $\beta^i = df^i$. The Hodge decomposition tells us that every 1-form ξ may be written as

$$\xi = df + \gamma,$$

where $\delta\gamma = 0$ and $\delta : \Omega^1(M, \mathbb{R}) \to C^\infty(M)$ is the codifferential operator.

The space $\mathrm{Imm}(M, \mathbb{R}^3)$ is formally a submanifold of $\Omega^1_+(M, \mathbb{R}^3)$, and thus by general submanifold geometry, we know that the geodesic equation on $\mathrm{Imm}(M, \mathbb{R}^3)$ will be given by

$$\frac{D}{dt}\frac{d}{dt}\alpha = \gamma, \qquad \alpha = d\Phi, \qquad \delta\gamma = 0.$$

Since $\delta\gamma = 0$, we know that $\star\gamma$ is an exact form, where $\star$ denotes the Hodge star operator. Then, there is a function p, unique up to a constant, such that $dp = \star\gamma$. We obtain

$$\Delta p = \delta dp = \delta\star\gamma = \star d\left(\frac{D}{dt}\frac{d}{dt}\alpha\right).$$

In coordinates (u, v) on M, the operator $\star d$ is given by:

$$\star d(f\, du + g\, dv) = \frac{g_u - f_v}{\varphi},$$

where φ is the volume form on M. From the geodesic equation on $\Omega^1_+(M, \mathbb{R}^3)$ with respect to the metric (3), as calculated in our previous paper [7], we know that the covariant derivative is given by

$$\frac{D}{dt}\frac{d\alpha}{dt} = \alpha_{tt} - \alpha_t(\alpha^T\alpha)^{-1}\alpha_t^T\alpha - \alpha_t\alpha^+\alpha_t + (\alpha_t\alpha^+)^T\alpha_t - \tfrac{1}{2}\,\mathrm{tr}(\alpha_t(\alpha^T\alpha)^{-1}\alpha_t^T)\alpha + \mathrm{tr}(\alpha_t\alpha^+)\alpha_t.$$

Since $d\alpha_{tt} = 0$, we obtain

$$\Delta p = \star d\Big(-\alpha_t(\alpha^T\alpha)^{-1}\alpha_t^T\alpha\Big) - \alpha_t\alpha^+\alpha_t + (\alpha_t\alpha^+)^T\alpha_t - \tfrac{1}{2}\,\mathrm{tr}(\alpha_t(\alpha^T\alpha)^{-1}\alpha_t^T)\alpha + \mathrm{tr}(\alpha_t\alpha^+)\alpha_t\Big).$$

Let $L = \alpha_t \alpha^+$. Applying the Hodge star operator to both sides, we see that Φ is a geodesic on $\mathrm{Imm}(M, \mathbb{R}^3)$ if and only if we have

$$\star \Delta p = \star\star d(\Omega d\Phi) = d\Omega \wedge d\Phi$$

where $\Omega = LL^T + L^2 - L^T L + \frac{1}{2}\mathrm{tr}(L^T L) - \mathrm{tr}(L)L$. Here, we emphasize that p and Φ are actually vector-valued functions, so these computations are done componentwise for each $i \in \{1, 2, 3\}$. In other words, we have

$$\star \Delta p_i = \sum_{j=1}^{3} d\Omega_{ij} \wedge d\Phi_j, \qquad i \in \{1, 2, 3\}.$$

Appendix B: Proofs

Proof of Theorem 2 In the following, we prove the correspondence between our split metric on the space $\Omega^1_+(M, \mathbb{R}^3)$ and the SRNF metric on the space of surfaces. Let $M_+(3, 2)$ be the space of 3×2 matrices with rank 2. Using the pointwise property of our metric, we will focus on the corresponding split metric on the matrix space $M_+(3, 2)$. For $a \in M_+(3, 2)$ and $v \in T_m M_+(3, 2)$, we decompose v into four parts

$$v = v_m + \frac{1}{2}\mathrm{tr}(a^+ v)a + v^\perp + v_0,$$

where

$$\begin{aligned} v_m &= \frac{1}{2}a(a^T a)^{-1}(a^T v + v^T a) - \frac{1}{2}\mathrm{tr}(a^+ v)a \\ v^\perp &= v - a(a^T a)^{-1}a^T v \\ v_0 &= \frac{1}{2}a(a^T a)^{-1}(a^T v - v^T a). \end{aligned}$$

The corresponding split metric on $M_+(3, 2)$ is then of the form:

$$\begin{aligned} &G_a^{\mathfrak{a},\mathfrak{b},\mathfrak{c},\mathfrak{d}}(v, v) \\ &\quad = \mathfrak{a}\langle v_m, v_m\rangle_a + \mathfrak{b}\left\langle \frac{1}{2}\mathrm{tr}(a^+ v)a, \frac{1}{2}\mathrm{tr}(a^+ v)a \right\rangle_a \\ &\qquad + \mathfrak{c}\langle v^\perp, v^\perp\rangle_a + \mathfrak{d}\langle v_0, v_0\rangle_a, \end{aligned} \tag{13}$$

Now consider the projection $\pi : M_+(3, 2) \to \mathrm{Sym}_+(2)$, $a \mapsto a^T a$. This projection is a Riemannian submersion, where $M_+(3, 2)$ carries metric (13) with choices of constants $(1, 1, 1, 1)$ and the space $\mathrm{Sym}_+(2)$ is equipped with the following metric:

$$\langle h, k\rangle_g^{\mathrm{Sym}} = \frac{1}{4}\mathrm{tr}(g^{-1}hg^{-1}k)\sqrt{\det(g)}.$$

The horizontal bundle with respect to the projection π is given by

$$\mathcal{H}_a = \{u \in M(3, 2) \mid ua^+ \in \mathrm{Sym}(n)\},$$

and the differential $d\pi$ induces an isometry

$$d\pi_a : \mathcal{H}_a \to T_{\pi(a)}\,\mathrm{Sym}_+(m).$$

It is easy to check that v_m and $\frac{1}{2}\mathrm{tr}(a^+ v)a$ are horizontal vectors.

Let $g = \pi(a) = a^T a$. By computation, we have

$$\mathrm{tr}(a^+ v) = \frac{1}{2}\mathrm{tr}(g^{-1} d\pi_a v)$$

and

$$\begin{aligned} d\pi_a(v_m) &= a^T v_m + v_m^T a = a^T v + v^T a - \mathrm{tr}(a^+ v)a^T a \\ &= d\pi_a v - \frac{1}{2}\mathrm{tr}\left(g^{-1} d\pi_a v\right) g. \end{aligned}$$

Therefore, the first term in (13) becomes

$$\begin{aligned} &\langle v_m, v_m\rangle_a \\ &\quad = \langle d\pi_a(v_m), d\pi_a(v_m)\rangle_{\pi(a)}^{\mathrm{Sym}} \\ &\quad = \left\langle d\pi_a v - \frac{1}{2}\mathrm{tr}\left(g^{-1} d\pi_a v\right) g, d\pi_a v - \frac{1}{2}\mathrm{tr}\left(g^{-1} d\pi_a v\right) g \right\rangle_g^{\mathrm{Sym}} \\ &\quad = \langle d\pi_a v, d\pi_a v\rangle_g^{\mathrm{Sym}} - \mathrm{tr}\left(g^{-1} d\pi_a v\right)\langle d\pi_a v, g\rangle_g^{\mathrm{Sym}} \\ &\qquad + \frac{1}{4}\mathrm{tr}^2\left(g^{-1} d\pi_a v\right)\langle g, g\rangle_g^{\mathrm{Sym}} \\ &\quad = \frac{1}{4}\mathrm{tr}\left(g^{-1} d\pi_a v g^{-1} d\pi_a v\right)\sqrt{\det(g)} \\ &\qquad - \frac{1}{8}\mathrm{tr}^2\left(g^{-1} d\pi_a v\right)\sqrt{\det(g)} \end{aligned}$$

and the second term becomes

$$\begin{aligned} \left\langle \frac{1}{2}\mathrm{tr}(a^+ v)a, \frac{1}{2}\mathrm{tr}(a^+ v)a \right\rangle_a &= \frac{1}{2}\mathrm{tr}^2(a^+ v)\sqrt{\det(a^T a)} \\ &= \frac{1}{8}\mathrm{tr}^2(g^{-1} d\pi_a v)\sqrt{\det(g)}. \end{aligned}$$

For the third term in (13), we consider the corresponding unit normal map on the space of matrices given by

$$\begin{aligned} n : M_+(3, 2) &\to \mathbb{R}^3 \\ a &\mapsto \frac{a_1 \times a_2}{|a_1 \times a_2|} = \frac{a_1 \times a_2}{\sqrt{\det(a^T a)}}, \end{aligned}$$

where a_1 and a_2 are the first and the second columns of a, respectively. For any tangent vector $u = \begin{pmatrix} u_1 & u_2 \end{pmatrix}$ at a, the

differential of n at a is

$$dn_a(u) = \frac{u_1 \times a_2 + a_1 \times u_2 - (a_1 \times a_2)\,\mathrm{tr}(a^+ u)}{\sqrt{\det(a^T a)}}.$$

It is easy to check that $aa^+ v$ is in the kernel of the differential dn_a, i.e.,

$$dn_a(v) = dn_a(v^\perp + aa^+ v) = dn_a(v^\perp).$$

Note that $\mathrm{tr}(a^+ v^\perp) = 0$, $aa^+ a_1 = a_1$ and $aa^+ a_2 = a_2$. Using the following identity for three-dimensional vectors b, c, d, e:

$$(b \times c) \cdot (d \times e) = b^T d c^T e - b^T e c^T d$$

and the formula for the inverse of $a^T a$:

$$(a^T a)^{-1} = \frac{1}{\det(a^T a)} \begin{pmatrix} a_2^T a_2 & -a_1^T a_2 \\ a_1^T a_2 & a_1^T a_1 \end{pmatrix},$$

we have

$$\begin{aligned}
&\langle dn_a v, dn_a v\rangle_{\mathbb{R}^3} = \langle dn_a v^\perp, dn_a v^\perp\rangle_{\mathbb{R}^3} \\
&= \frac{1}{\det(a^T a)} \langle v_1^\perp \times a_2 + a_1 \times v_2^\perp, v_1^\perp \times a_2 + a_1 \times v_2^\perp\rangle_{\mathbb{R}^3} \\
&= \frac{1}{\det(a^T a)} \big[\left(v_1^T v_1 - v_1^T aa^+ v_1\right) a_2^T a_2 \\
&\quad - 2\left(v_1^T v_2 - v_1^T aa^+ v_2\right) a_1^T a_2 + \left(v_2^T v_2 - v_2^T aa^+ v_2\right) a_1^T a_1 \big],
\end{aligned}$$

where $v_1^\perp$, $v_2^\perp$ are the first and the second columns of $v^\perp$ and v_1, v_2 are the first and the second columns of v, respectively. It follows that

$$\begin{aligned}
&\left\langle v^\perp, v^\perp \right\rangle_a \sqrt{\det(a^T a)} = \mathrm{tr}(v^\perp (a^T a)^{-1} (v^\perp)^T) \det(a^T a) \\
&= \left(\mathrm{tr}(v(a^T a)^{-1} v^T) - \mathrm{tr}(aa^+ v (a^T a)^{-1} v^T)\right) \det(a^T a) \\
&= \left(\mathrm{tr}(v^T v (a^T a)^{-1}) - \mathrm{tr}(v^T aa^+ v (a^T a)^{-1})\right) \det(a^T a) \\
&= \mathrm{tr}\left(\begin{pmatrix} v_1^T (I - aa^+) v_1 & v_1^T (I - aa^+) v_2 \\ v_1^T (I - aa^+) v_2 & v_2^T (I - aa^+) v_2 \end{pmatrix} \begin{pmatrix} a_2^T a_2 & -a_1^T a_2 \\ a_1^T a_2 & a_1^T a_1 \end{pmatrix} \right) \\
&= \left(v_1^T v_1 - v_1^T aa^+ v_1\right) a_2^T a_2 - 2\left(v_1^T v_2 - v_1^T aa^+ v_2\right) a_1^T a_2 \\
&\quad + \left(v_2^T v_2 - v_2^T aa^+ v_2\right) a_1^T a_1 \\
&= \langle dn_a v, dn_a v\rangle_{\mathbb{R}^3} \det(a^T a),
\end{aligned}$$

that is,

$$\left\langle v^\perp, v^\perp \right\rangle_a = \langle dn_a v, dn_a v\rangle_{\mathbb{R}^3} \sqrt{\det(g)}.$$

Therefore, the split metric (13) on $M_+(3,2)$ can be rewritten as

$$\begin{aligned}
&G_a^{\mathfrak{a},\mathfrak{b},\mathfrak{c},\mathfrak{d}}(v, v) \\
&= \mathfrak{a}\left(\frac{1}{4}\,\mathrm{tr}\left(g^{-1} d\pi_a v g^{-1} d\pi_a v\right) - \frac{1}{8}\,\mathrm{tr}^2\left(g^{-1} d\pi_a v\right)\right)\sqrt{\det(g)} \\
&\quad + \frac{\mathfrak{b}}{8}\,\mathrm{tr}^2\left(g^{-1} d\pi_a v\right)\sqrt{\det(g)} + \mathfrak{c}\langle dn_a v, dn_a v\rangle_{\mathbb{R}^3}\sqrt{\det(g)} \\
&\quad + \mathfrak{d}\langle v_0, v_0\rangle_a.
\end{aligned}$$

Now it is easy to see that the first three terms give rise to the formula of the full elastic metric on the space of surfaces for $A = \mathfrak{a}/4$, $B = (\mathfrak{b} - \mathfrak{a})/8$, $C = \mathfrak{c}$ and the SRNF metric corresponds to the split metric (4) with constants $(0, \frac{1}{2}, 1, 0)$. □

Proof of Theorem 3 We first perform the computation in spherical coordinates $(\theta, \phi) \in [0, 2\pi] \times [0, \pi]$. Denote the usual spherical coordinate orthonormal basis by

$$\begin{aligned}
e_1 &= \langle \sin\phi\cos\theta, \sin\phi\sin\theta, \cos\phi\rangle, \\
e_2 &= \langle \cos\phi\cos\theta, \cos\phi\sin\theta, -\sin\phi\rangle, \\
e_3 &= \langle -\sin\theta, \cos\theta, 0\rangle.
\end{aligned}$$

We have the following formulas for the partial derivatives:

$$\begin{aligned}
&\partial_\phi e_1 = e_2, \qquad \partial_\phi e_2 = -e_1, \qquad \partial_\phi e_3 = 0, \\
&\partial_\theta e_1 = \sin\phi e_3, \qquad \partial_\theta e_2 = \cos\phi e_3, \\
&\partial_\theta e_3 = -\sin\phi e_1 - \cos\phi e_2.
\end{aligned} \tag{14}$$

We also note that the covariant derivatives are given by

$$\begin{aligned}
&\nabla_{e_2} e_2 = 0, && \nabla_{e_2} e_3 = 0 \\
&\nabla_{e_3} e_2 = \cot\phi\, e_3, && \nabla_{e_3} e_3 = -\cot\phi\, e_2.
\end{aligned} \tag{15}$$

Write

$$U(\theta, \phi) = u(\theta, \phi) e_2(\theta, \phi) + v(\theta, \phi) e_3(\theta, \phi).$$

For a real parameter t, we consider the following map $W\colon S^2 \to \mathbb{R}^3$ given in coordinates by

$$\begin{aligned}
W(\theta, \phi) &= e_1(\theta, \phi) + tU(\theta, \phi) \\
&= e_1(\theta, \phi) + tu(\theta, \phi) e_2(\theta, \phi) + tv(\theta, \phi) e_3(\theta, \phi).
\end{aligned}$$

Then, $\eta = W/|W|$.

Note that in order for η to be a diffeomorphism, we require that the Jacobian determinant be nonzero; it is given by

$$\mathrm{Jac}(\eta) = \frac{1}{\sin\phi} \left| \frac{\partial \eta}{\partial \phi} \times \frac{\partial \eta}{\partial \theta} \right|.$$

Observe that

$$\begin{aligned}
\eta_\phi &= \frac{1}{|W|}\left(W_\phi - \frac{W \cdot W_\phi}{|W|^2} W\right) = \frac{1}{|W|} P_{W^\perp}(W_\phi), \\
\eta_\theta &= \frac{1}{|W|}\left(W_\theta - \frac{W \cdot W_\theta}{|W|^2} W\right) = \frac{1}{|W|} P_{W^\perp}(W_\theta).
\end{aligned}$$

Since η_ϕ and η_θ are both perpendicular to W, we know that $\eta_\phi \times \eta_\theta$ is parallel to W; thus, we obtain the formula

$$\begin{aligned}\mathrm{Jac}(\eta) &= \frac{1}{\sin\phi |W|^2}\left|P_{W^\perp}(W_\phi)\times P_{W^\perp}(W_\theta)\right| \\ &= \frac{1}{\sin\phi |W|^3}\left|W\cdot\left(P_{W^\perp}(W_\phi)\times P_{W^\perp}(W_\theta)\right)\right| \\ &= \frac{1}{\sin\phi |W|^3}\left|W\cdot\left(W_\phi\times W_\theta\right)\right|,\end{aligned}$$

using the cyclic invariance of the scalar triple product and the fact that $W \times P_{W^\perp}(V) = W \times V$ for any vector V.

Since $W = e_1 + tU$ for the vector field $U = ue_2 + ve_3$, it is straightforward to compute using (14)-(15) that

$$\begin{aligned}W_\phi &= e_2 + tU_\phi = e_2 + t\nabla_{e_2}U - tue_1, \\ \frac{W_\theta}{\sin\phi} &= e_3 + \frac{t}{\sin\phi}U_\theta = e_3 + t\nabla_{e_3}U - tve_1,\end{aligned}$$

Let $m_1 = u_\phi$, $m_2 = v_\phi$, $m_3 = \frac{u_\theta - v\cos\phi}{\sin\phi}$, $m_4 = \frac{v_\theta + u\cos\phi}{\sin\phi}$. We have by (15) that

$$\nabla_{e_2}U = m_1e_2 + m_2e_3, \qquad \nabla_{e_3}U = m_3e_2 + m_4e_3,$$

which we abbreviate by

$$M := \nabla U = \begin{pmatrix} m_1 & m_2 \\ m_3 & m_4\end{pmatrix}.$$

Thus, the Jacobian is nonzero if and only if the following determinant is nonzero:

$$D = \left|W\cdot\left(W_\phi\times W_\theta\right)\right| = \begin{vmatrix} 1 & tu & tv \\ -tu & 1+tm_1 & tm_2 \\ -tv & tm_3 & 1+tm_4\end{vmatrix}. \tag{16}$$

Expanding the determinant (16) along the first column, then it is given by

$$D = \det(1+tM) + t^2\langle JU, (1+tM)JU\rangle,$$

where $J = \begin{pmatrix} 0 & -1 \\ 1 & 0\end{pmatrix}$.

Let $\overline{M} = \frac{1}{2}(M + M^T)$ denote the symmetrization of M, and let $\lambda_1 \le \lambda_2$ denote the real eigenvalues of $\overline{M}$. Then, $\mathrm{tr}\, M = \mathrm{tr}\,\overline{M}$ and $\det M = \det\overline{M} + \frac{1}{4}(m_2 - m_3)^2$, so that

$$\det(1+tM) \ge \det(1+t\overline{M}) = (1+\lambda_1 t)(1+\lambda_2 t).$$

Since J is a rotation, we have

$$\begin{aligned}\langle JU, (1+tM)JU\rangle &= \langle JU, (1+t\overline{M})JU\rangle \\ &\ge (1+\lambda_1 t)|JU|^2 \\ &= (1+\lambda_1 t)|U|^2.\end{aligned}$$

Thus,

$$D \ge (1+\lambda_1 t)(1+\lambda_2 t + |U|^2t^2).$$

For sufficiently small t, we know $(1+\lambda_1 t)$ is positive, and since $\lambda_1 \le \lambda_2$, we obtain

$$D \ge (1+\lambda_1 t)^2$$

Thus, $1+\lambda_1 t > 0$ is a sufficient condition for positivity of D, and this happens as long as $|t| < \frac{1}{|\lambda_1|}$. It is easy to compute that

$$\lambda_1 = \frac{m_1 + m_4 - \sqrt{(m_1-m_4)^2 + (m_2+m_3)^2}}{2}.$$

In particular, $m_1 + m_4 = \mathrm{tr}\,(\nabla U) = \mathrm{div}\, U$, and by the divergence theorem, we know the integral of $m_1 + m_4$ over S^2 is zero, and in particular $m_1 + m_4$ is either identically zero or changes sign on S^2. Since t is nonnegative, we therefore are concerned about the most negative that $\lambda_1(x)$ can be:

$$1 + \lambda_1(x)t \ge 1 + t\inf_{x\in S^2}\lambda_1(x) = 1 - t\sup_{p\in S^2}(-\lambda_1(x)) \ge 0,$$

which is equivalent to

$$t < \frac{2}{\sup\limits_{p\in S^2} -(m_1+m_4) + \sqrt{(m_1-m_4)^2 + (m_2+m_3)^2}}.$$

This is clearly (9). □

References

1. Abe, K., Erbacher, J.: Isometric immersions with the same gauss map. Math. Ann. **215**(3), 197–201 (1975)
2. Allen, B., Curless, B., Popović, Z.: The space of human body shapes: reconstruction and parameterization from range scans. ACM Trans. Graph. **22**(3), 587–594 (2003)
3. Bauer, M., Bruveris, M., Charon, N., Møller-Andersen, J.: A relaxed approach for curve matching with elastic metrics. To appear in ESAIM: COCV (2018)
4. Bauer, M., Bruveris, M., Michor, P.W.: Overview of the geometries of shape spaces and diffeomorphism groups. J. Math. Imaging Vis. **50**(1–2), 60–97 (2014)
5. Bauer, M., Harms, P., Michor, P.W.: Sobolev metrics on shape space of surfaces. J. Geom. Mech. **3**(4), 389–438 (2011)
6. Bauer, M., Harms, P., Michor, P.W.: Sobolev metrics on shape space, ii: weighted sobolev metrics and almost local metrics. J. Geom. Mech. **4**(4), 365–383 (2012)
7. Bauer, M., Klassen, E., Preston, S.C., Su, Z.: A diffeomorphism-invariant metric on the space of vector-valued one-forms. arXiv:1812.10867 (2018)
8. Bronstein, A.M., Bronstein, M.M., Kimmel, R.: Numerical Geometry of Non-Rigid Shapes. Springer, Berlin (2008)

9. Bruveris, M., Michor, P.W., Mumford, D.: Geodesic completeness for sobolev metrics on the space of immersed plane curves. In: Guralnick, R. (ed.) Forum of Mathematics, Sigma, vol. 2. Cambridge University Press (2014)
10. Celledoni, E., Eslitzbichler, M., Schmeding, A.: Shape analysis on Lie groups with applications in computer animation. J. Geom. Mech. **8**(3), 273–304 (2015)
11. Cervera, V., Mascaro, F., Michor, P.W.: The action of the diffeomorphism group on the space of immersions. Differ. Geom. Appl. **1**(4), 391–401 (1991)
12. Cury, C., Glaunes, J.A., Colliot, O.: Template estimation for large database: a diffeomorphic iterative centroid method using currents. In: International Conference on Geometric Science of Information, pp. 103–111. Springer (2013)
13. Fletcher, R.: Practical Methods of Optimization. Wiley, Amsterdam (2013)
14. Grenander, U., Miller, M.I.: Computational anatomy: an emerging discipline. Q. Appl. Math. **56**(4), 617–694 (1998)
15. Hasler, N., Stoll, C., Sunkel, M., Rosenhahn, B., Seidel, H.P.: A statistical model of human pose and body shape. In: Hauser, H., Benes, B (eds.) Computer Graphics Forum, vol. 28, pp. 337–346. Wiley Online Library (2009)
16. Heeren, B., Rumpf, M., Wardetzky, M., Wirth, B.: Time-discrete geodesics in the space of shells. In: Hauser, H., Benes, B (eds.) Computer Graphics Forum, vol. 31, pp. 1755–1764. Wiley Online Library (2012)
17. Jermyn, I., Kurtek, S., Laga, H., Srivastava, A.: Elastic shape analysis of three-dimensional objects. Synth. Lect. Comput. Vis. **7**, 1–185 (2017)
18. Jermyn, I.H., Kurtek, S., Klassen, E., Srivastava, A.: Elastic shape matching of parameterized surfaces using square root normal fields. Comput. Vis. ECCV **2012**, 804–817 (2012)
19. Kilian, M., Mitra, N.J., Pottmann, H.: Geometric modeling in shape space. In: ACM Transactions on Graphics (TOG), vol. 26, p. 64. ACM (2007)
20. Klassen, E., Michor, P.W.: Closed surfaces with different shapes that are indistinguishable by the srnf. arXiv:1910.10804. (2019)
21. Kühnel, L., Sommer, S., Arnaudon, A.: Differential geometry and stochastic dynamics with deep learning numerics. Appl. Math. Comput. **356**, 411–437 (2019)
22. Kurtek, S., Klassen, E., Ding, Z., Jacobson, W., Jacobson, S., Avison, J.L.J.M., Srivastava, A.: Parameterization-invariant shape comparisons of anatomical surfaces. IEEE Trans. Med. Imaging **30**(3), 849–858 (2011)
23. Kurtek, S., Needham, T.: Simplifying transforms for general elastic metrics on the space of plane curves. arXiv preprint arXiv:1803.10894 (2018)
24. Kurtek, S., Srivastava, A., Klassen, E., Laga, H.: Landmark-guided elastic shape analysis of spherically-parameterized surfaces. In: Hauser, H., Benes, B (eds.) Computer Graphics Forum, vol. 32, pp. 429–438. Wiley Online Library (2013)
25. Laga, H., Xie, Q., Jermyn, I.H., Srivastava, A.: Numerical inversion of srnf maps for elastic shape analysis of genus-zero surfaces. IEEE Trans. Pattern Anal. Mach. Intell. **39**(12), 2451–2464 (2017)
26. Mio, W., Srivastava, A., Joshi, S.: On shape of plane elastic curves. Int. J. Comput. Vis. **73**(3), 307–324 (2007)
27. Praun, E., Hoppe, H.: Spherical parametrization and remeshing. In: ACM Transactions on Graphics (TOG), vol. 22, pp. 340–349. ACM (2003)
28. Srivastava, A., Klassen, E., Joshi, S.H., Jermyn, I.H.: Shape analysis of elastic curves in euclidean spaces. IEEE Trans. Pattern Anal. Mach. Intell. **33**(7), 1415–1428 (2011)
29. Srivastava, A., Klassen, E.P.: Functional and Shape Data Analysis. Springer, Berlin (2016)
30. Su, J., Kurtek, S., Klassen, E., Srivastava, A.: Statistical analysis of trajectories on Riemannian manifolds: bird migration, hurricane tracking and video surveillance. Ann. Appl. Stat. **8**(1), 530–552 (2014)
31. Su, Z., Klassen, E., Bauer, M.: Comparing curves in homogeneous spaces. In: Slovák, J. (ed.) Differential Geometry and its Applications, vol. 60, pp. 9–32. Elsevier (2018)
32. Tumpach, A.B.: Gauge invariance of degenerate riemannian metrics. Notices of the AMS **63**(4), 342–350 (2016)
33. Tumpach, A.B., Drira, H., Daoudi, M., Srivastava, A.: Gauge invariant framework for shape analysis of surfaces. IEEE Trans. Pattern Anal. Mach. Intell. **38**(1), 46–59 (2015)
34. Younes, L.: Computable elastic distances between shapes. SIAM J. Appl. Math. **58**(2), 565–586 (1998)
35. Younes, L., Michor, P.W., Shah, J.M., Mumford, D.B.: A metric on shape space with explicit geodesics. Rendiconti Lincei-Matematica e Applicazioni **19**(1), 25–57 (2008)
36. Zhang, Z., Su, J., Klassen, E., Le, H., Srivastava, A.: Video-based action recognition using rateinvariant analysis of covariance trajectories. arXiv:1503.06699 (2015)

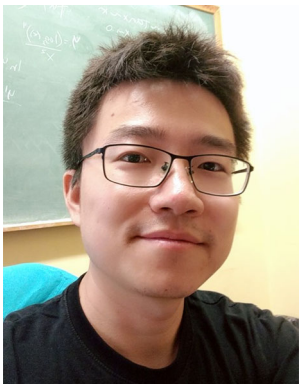

Zhe Su is a Ph.D. candidate in Mathematics at Florida State University. His research interests include differential geometry, shape analysis and its applications.

Martin Bauer received his Ph.D. in Mathematics from the University of Vienna in 2010 under the supervision of Peter W. Michor and the Habilitation (venia docendi) in 2015. Since 2016, he is an Assistant Professor at Florida State University. His research interests include infinite-dimensional Riemannian geometry, shape analysis and geometric mechanics.

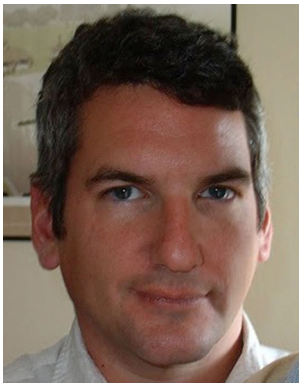

Stephen C. Preston received a Ph.D. in Mathematics from SUNY Stony Brook in 2002 under David G. Ebin. He has worked at the University of Pennsylvania and the University of Colorado in Boulder. Since 2016, he has been at Brooklyn College and the CUNY Graduate Center and has been Chair of the Mathematics Department since 2018. His research is focused on partial differential equations and Riemannian geometry.

Hamid Laga received the Ph.D. degrees in Computer Science from Tokyo Institute of Technology in 2006. He is currently an Associate Professor at Murdoch University (Australia) and an Adjunct Associate Professor with the Phenomics and Bioinformatics Research Centre (PBRC) of the University of South Australia. His research interests span various fields of machine learning, computer vision, computer graphics and pattern recognition, with a special focus on the 3D reconstruction, modeling and analysis of static and deformable 3D objects, and on image analysis and big data in agriculture and health. He is the recipient of multiple awards including the Best Paper Awards at SGP2017, DICTA2012 and SMI2006.

Eric Klassen received his Ph.D. in Mathematics from Cornell University in 1987. After completing a postdoc at Caltech, he became a faculty member at Florida State University. His research interests have included knot theory, gauge theory, Riemann surfaces and shape analysis. He is coauthor (with Anuj Srivastava) of the book "Functional and Shape Data Analysis" (Springer, 2016).